Spin Delocalization in Electron-Rich Iron(III) Piano-Stool σ-Acetylides. An Experimental (NMR) and Theoretical (DFT) Investigation

Frédéric Paul,*,† Grégory da Costa,‡ Arnaud Bondon,*,‡ Nicolas Gauthier,† Sourisak Sinbandhit,§ Loic Toupet,⊥ Karine Costuas,† Jean-François Halet,† and Claude Lapinte†

Sciences Chimiques de Rennes, UMR 6226 CNRS, Université de Rennes 1, Campus de Beaulieu, 35042 Rennes Cedex, France, RMN-ILP, UMR 6026 CNRS, Université de Rennes 1, IFR 140−PRISM, CS 34317, Campus de Villejean, 35043 Rennes Cedex, France, CRMPO, Université de Rennes 1, Campus de Beaulieu, 35042 Rennes Cedex, France, and Groupe Matière Condensée et Matériaux, UMR 6626 CNRS, Université de Rennes I, Campus de Beaulieu, 35042 Rennes Cedex, France

Received October 26, 2006

Several paramagnetic electron-rich Fe(III) mononuclear arylacetylide complexes of formula [(η^2-dppe)(η^5-C_5Me_5)Fe(C≡C−Ar)]$^+$ in which Ar represents a functional aryl group were studied by means of multinuclear NMR. All signals detected for the various nuclei were assigned. Hyperfine coupling constants for selected nuclei of the arylacetylide ligand were derived from ^{1}H or ^{19}F NMR contact shifts. These NMR data are diagnostic of a metal-centered unpaired electron partly residing in a π molecular orbital on the arylacetylide ligand, in line with DFT computations. We show here that the ^{1}H NMR paramagnetic shifts of the ortho (H_1) and meta (H_2) arylacetylide protons convey decisive information on the charge distribution in the aryl ring. Estimates of the relaxation rates of the unpaired electron were also derived from half-widths of the ^{1}H NMR signals. Finally, line-broadening studies of Fe(II)/Fe(III) mixtures allowed extracting the self-exchange rates for several redox couples among these complexes. The self-exchange rates appear slightly substituent dependent and are apparently larger for compounds with electron-withdrawing substituents on the aryl ring. Reorganization energies of ca. 4000 cm^{-1} could be derived for these outer-sphere electron-transfer processes.

Introduction

These last decades, in the emerging field of molecular electronics,[1] mono- or polynuclear organometallic complexes featuring carbon-rich ligands and stable over several redox states have aroused a lot of academic interest as potential redox-switchable components,[2−4] not only as single molecule devices but also as molecular precursors for attaining new materials with specifically tailored properties.[3f,5] A constant feature usually observed with such compounds is the strong dependence of their electronic structure and properties on the redox state of the appended metal center.[3a,6,7] Thus, in suitably designed carbon-rich compounds, it has been shown in several instances that the overall enhancement (or inhibition) of a given electronic

* Corresponding authors. Tel: 33 (0)2 23 23 59 62. Fax: 33 (0)2 23 23 56 37. E-mail: frederic.paul@univ-rennes1.fr. Tel: 33 (0)2 23 23 65 61. Fax: 33 (0)2 23 23 46 06. E-mail: arnaud.bondon@univ-rennes1.fr.

† UMR CNRS 6226: Sciences Chimiques de Rennes.

‡ UMR CNRS 6026: RMN-ILP.

§ CRMPO.

⊥ UMR CNRS 6626: Groupe Matière Condensée et Matériaux.

(1) (a) Robertson, N.; Mc. Gowan, G. A. *Chem. Soc. Rev.* **2003**, *32*, 96−103. (b) Caroll, R. L.; Gorman, C. B. *Angew. Chem., Int. Ed. Engl.* **2002**, *41*, 4379−4400. (c) Tour, J. M. *Acc. Chem. Res.* **2000**, *33*, 791−803.

(2) (a) Gao, L.-B.; Liu, S.-H.; Zhang, L.-Y.; Shi, L.-X.; Chen, Z.-N. *Organometallics* **2006**, *25*, 506−512. (b) Gao, L.-B.; Zhang, L.-Y.; Shi, L.-X.; Chen, Z.-N. *Organometallics* **2005**, *24*, 1678−1684. (c) Qi, H.; Ghupta, A.; Noll, B. C.; Snider, G. L.; Lu, Y.; Lent, C. S.; Fehlner, T. P. *J. Am. Chem. Soc.* **2005**, *127*, 15218−15227. (d) Blum, A. S.; Ren, T.; Parish, D. A.; Trammell, S. A.; Moore, M. H.; J. G. Kushmerick; Xu, G.-L.; Deschamps, J. R.; Polack, S. K.; Shashidar, R. *J. Am. Chem. Soc.* **2005**, *127*, 10010−10011. (e) Wong, W.-Y.; Che, C.-M.; Chan, M. C. W.; Han, J.; Leung, K.-H.; Phillips, D. L.; Wong, K.-Y.; Zhu, N. *J. Am. Chem. Soc.* **2005**, *127*, 13997−14007. (f) Xu, G.-L.; Crutchley, R. J.; DeRosa, M. C.; Pan, Q.-J.; Zhang, H.-X.; Wang, X.; Ren, T. *J. Am. Chem. Soc.* **2005**, *127*, 13354−13365. (g) Hu, Q. Y.; Lu, W. X.; Tang, H. D.; Sung, H. H. Y.; Wen, T. B.; Williams, I. D.; Wong, G. K. L.; Lin, Z.; Jia, G. *Organometallics* **2005**, *24*, 3966−3973. (h) Venkatesan, K.; Blacque, O.; Fox, T.; Alfonso, M.; Schmalle, H. W.; Berke, H. *Organometallics* **2004**, *23*, 1183−1186. (i) Fraysse, S.; Coudret, C.; Launay, J.-P. *J. Am. Chem. Soc.* **2003**, *125*, 5880−5888. (j) Naklicki, M. L.; White, C. A.; Plante, L. L.; Evans, C. E. B.; Crutchley, R. J. *Inorg. Chem.* **1998**, *37*, 1880−1885.

(3) (a) Ren, T. *Organometallics* **2005**, *24*, 4854−4870. (b) Powell, C. E.; Humphrey, M. G. *Coord. Chem. Rev.* **2004**, *248*, 725−756. (c) Rigaut, S.; Touchard, D.; Dixneuf, P. H. *Coord. Chem. Rev.* **2004**, *248*, 1585−1601. (d) Bruce, M. I.; Low, P. J. *Adv. Organomet. Chem.* **2004**, *50*, 179−444. (e) Ceccon, A.; Santi, S.; Orian, L.; Bisello, A. *Coord. Chem. Rev.* **2004**, *248*, 683−724. (f) Long, N. J.; Williams, C. K. *Angew. Chem., Int. Ed.* **2003**, *42*, 2586−2617. (g) Yam, V. W.-W. *Acc. Chem. Res.* **2002**, *35*, 555−563.

(4) (a) Cifuentes, M. P.; Humphrey, M. G.; Morall, J. P.; Samoc, M.; Paul, F.; Roisnel, T.; Lapinte, C. *Organometallics* **2005**, *24*, 4280−4288. (b) Hurst, S. K.; Cifuentes, M. P.; Morrall, J. P. L.; Lucas, N. T.; Whittal, I. R.; Humphrey, M. G.; Asselberghs, I.; Persoons, A.; Samoc, M.; Luther-Davies, B.; Willis, A. C. *Organometallics* **2001**, *20*, 4664−4675. (c) Powell, C. E.; Humphrey, M. G.; Cifuentes, M. P.; Morall, J. P.; Samoc, M.; Luther-Davies, B. *J. Phys. Chem. A* **2003**, *107*, 11264−11266.

(5) (a) Schwab, P. F. H.; Smith, J. R.; Michl, J. *Chem. Rev.* **2005**, *105*, 1197−1279. (b) Schwab, P. F. H.; Levin, M. D.; Michl, J. *Chem. Rev.* **1999**, *99*, 1863−1933. (c) Fillaut, J.-L.; Perruchon, J.; Blanchard, P.; Roncali, J.; Gohlen, S.; Allain, M.; Migalska-Zalas, A.; Kityk, I. V.; Sahraoui, B. *Organometallics* **2005**, *24*, 687−695. (d) Szafert, S.; Gladysz, J. A. *Chem. Rev.* **2003**, *103*, 4175−4205.

(6) (a) Paul, F.; Lapinte, C. *Coord. Chem. Rev.* **1998**, *178/180*, 427−505. (b) Paul, F.; Lapinte, C. In *Unusual Structures and Physical Properties in Organometallic Chemistry*; Gielen, M., Willem, R., Wrackmeyer, B., Eds.; Wiley & Sons, Ldt: San-Francisco, 2002; pp 219−295.

(7) Crutchley, R. J. *Adv. Inorg. Chem.* **1994**, *41*, 273−325.

10.1021/om060989j CCC: $37.00
Publication on Web 01/17/2007

Chart 1

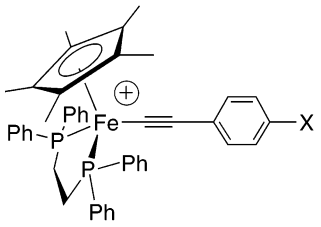

X

1a$^+$: NO_2 **1f**$^+$: H
1b$^+$: CN **1g**$^+$: Me
1c$^+$: CF_3 **1h**$^+$: OMe
1d$^+$: F **1i**$^+$: NH_2
1e$^+$: Br **1j**$^+$: NMe_2

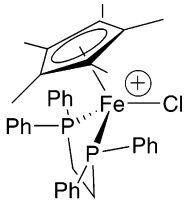

2$^+$

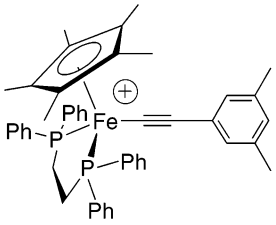

3a$^+$

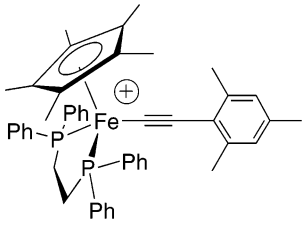

3b$^+$

property such as fluorescence or nonlinear optical (NLO) activity can be achieved upon variation of the redox state of the metal center.[4,8−9]

For several years now, our group has focused on electron-rich iron piano-stool acetylide complexes featuring "(η^2-dppe)(η^5-C_5Me_5)Fe(C≡C)−" fragments (dppe = 1,2-bis(diphenylphosphino)ethane).[10] Polynuclear architectures of this kind have revealed an appealing potential to realize molecular-scaled wires or magnets,[6,10] and also redox-switchable photonic devices, especially when associated with arylethynyl ligands.[4a,8] Now, a prerequisite to design more efficient molecular assemblies possessing similar properties is to obtain a good understanding of the electronic perturbation induced by the iron center on the nearby carbon-rich ligand, depending on its redox state. To date, this end-group, as well as its Ru(II) analogue,[11] was conclusively demonstrated to behave as an electron-releasing group resembling a methoxy or amino substituent in the closed-shell Fe(II) state.[12−14] Its electronic behavior is however less well defined in the open-shell Fe(III) state.[15] Up to now, UV−visible−NIR and ESR investigations have clearly shown that mononuclear Fe(III) model complexes such as **1a**−**j**[PF_6] (Chart 1) were dominantly metal-centered $S = 1/2$ radical cations.[6] In addition, DFT calculations on computationally simpler models have suggested that significant delocalization of the electronic vacancy takes place on the arylacetylide ligand in compounds featuring strongly electron-releasing substituents.[15] If experimentally confirmed, this theoretical prediction constitutes a very important result for better understanding the unexpectedly large through-bridge exchange coupling sometimes observed in related polynuclear Fe(III) assemblies.[6b,10c,16] Unfortunately, no direct experimental confirmation of these theoretical predictions could be obtained to date. Indeed, ESR measurements, which usually provide estimates of the spin delocalization in a straightforward way, proved useless in that respect, since no (super)hyperfine structures were observed on the spectra recorded with frozen solutions of **1a**−**j**[PF_6], due to the fast electronic relaxation of these Fe(III) samples.[15]

Under such circumstances, in favorable cases, it is well known that NMR spectroscopy can allow determination of hyperfine couplings, providing not only their magnitude but also their sign.[17,18] We therefore decided to initiate a NMR study of the known paramagnetic compounds **1a**−**j**[PF_6] and **2**[PF_6], and also of the new paramagnetic **3a,b**[PF_6] complexes in which the arylacetylide has been "tagged" with methyl groups. Our first objective was to assign all the observable signals and, if possible, to *empirically* map the spin delocalization on the arylacetylide ligand in **1a**−**j**[PF_6] depending on the X substituent's nature. A second objective was then to compare experimental (NMR) with theoretical (DFT) estimates of the spin delocalization in these compounds, in order to determine the consistency of DFT calculations with experiment.

Much to our surprise, while comparing our results with previous investigations, we realized that although ^{1}H NMR had often been used as a convenient experimental tool to reveal or study (para)magnetism in related mono- or polynuclear organometallic complexes with carbon-rich ligands,[10,19−23] only

(8) (a) Wong, K. M.-C.; Lam, S. C.-F.; Ko, C.-C.; Zhu, N.; Yam, V. W.-W.; Roué, S.; Lapinte, C.; Fathallah, S.; Costuas, K.; Kahlal, S.; Halet, J.-F. *Inorg. Chem.* **2003**, *42*, 7086−7097. (b) Paul, F.; Costuas, K.; Ledoux, I.; Deveau, S.; Zyss, J.; Halet, J.-F.; Lapinte, C. *Organometallics* **2002**, *21*, 5229−5235. (c) Weyland, T.; Ledoux, I.; Brasselet, S.; Zyss, J.; Lapinte, C. *Organometallics* **2000**, *19*, 5235−5237.

(9) For an inorganic example, see also: Coe, B. J.; Houbrechts, S.; Asselberghs, I.; Persoons, A. *Angew. Chem., Int. Ed.* **1999**, *38*, 366−368.

(10) (a) Ibn Ghazala, S.; Paul, F.; Toupet, L.; Roisnel, T.; Hapiot, P.; Lapinte, C. *J. Am. Chem. Soc.* **2006**, *128*, 2463−2476. (b) de Montigny, F.; Argouarch, G.; Costuas, K.; Halet, J.-F.; Roisnel, T.; Toupet, L.; Lapinte, C. *Organometallics* **2005**, *24*, 4558−4572. (c) Bruce, M. I.; Low, P. J.; Hartl, F.; Humphrey, P. A.; de Montigny, F.; Jevric, M.; Lapinte, C.; G. J. Perki, S.; Roberts, R. L.; Skelton, B. W.; White, A. H. *Organometallics* **2005**, *24*, 5241−5255. (d) Paul, F.; Meyer, W.; Jiao, H.; Toupet, L.; Gladysz, J. A.; Lapinte, C. *J. Am. Chem. Soc.* **2000**, *122*, 9405−9414. (e) Le Stang, S.; Paul, F.; Lapinte, C. *Organometallics* **2000**, *19*, 1035−1043. (f) Le Narvor, N.; Toupet, L.; Lapinte, C. *J. Am. Chem. Soc.* **1995**, *117*, 7129−7138.

(11) Paul, F.; Ellis, B. J.; Bruce, M. I.; Toupet, L.; Roisnel, T.; Costuas, K.; Halet, J.-F.; Lapinte, C. *Organometallics* **2006**, *25*, 649−665.

(12) Costuas, K.; Paul, F.; Toupet, L.; Halet, J.-F.; Lapinte, C. *Organometallics* **2004**, *23*, 2053−2068.

(13) Paul, F.; Mevellec, J.-Y.; Lapinte, C. *J. Chem. Soc., Dalton Trans.* **2002**, 1783−1790.

(14) Denis, R.; Toupet, L.; Paul, F.; Lapinte, C. *Organometallics* **2000**, *19*, 4240−4251.

(15) Paul, F.; Toupet, L.; Thépot, J.-Y.; Costuas, K.; Halet, J.-F.; Lapinte, C. *Organometallics* **2005**, *24*, 5464−5478.

(16) Roué, S.; Le Stang, S.; Toupet, L.; Lapinte, C. *C. R. Chim.* **2003**, *6*, 353−366.

(17) Bertini, I.; Luchinat, C. *NMR of Paramagnetic Molecules in Biological Systems*; The Benjamin/Cummings Publishing Co.: Menlo Park, CA, 1986.

(18) McConnell, H. M.; Chesnut, D. B. *J. Chem. Phys.* **1958**, *28*, 107−117.

(19) Bruce, M.; Costuas, K.; Davin, T.; Ellis, B. J.; Halet, J.-F.; Lapinte, C.; Low, P. J.; Smith, M. E.; Skelton, B. W.; Toupet, L.; White, A. H. *Organometallics* **2005**, *24*, 3864−3881.

Scheme 1. (a) Ar = 3,5-Xyl and (b) Ar = 2,4,5-Mes

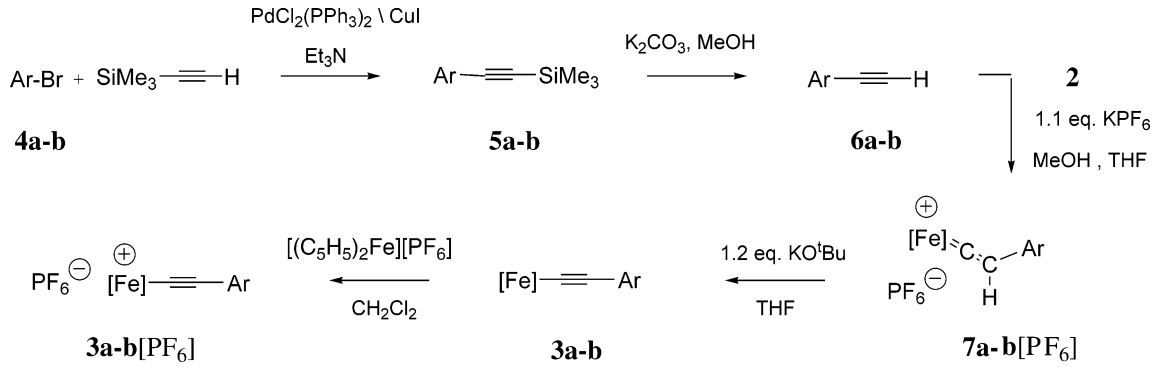

seldomly was a complete assignment of the observed signals provided.[21,23−26] More specifically with mononuclear acetylide complexes, a complete multinuclear NMR study aimed at assessing the importance of spin delocalization was conducted only once, to our knowledge,[26] and not with electron-rich aryl acetylides. This prompted us to communicate the present contribution, which usefully complements previous ^{1}H NMR studies made on **2**[PF_6] and **1f**[PF_6] (Chart 1).[21,22] Before discussing the NMR results, we will start by (i) briefly giving the synthesis and characterization of the new complexes **3a**[PF_6] and **3b**[PF_6]. We will next (ii) report and assign the ^{1}H, ^{13}C, ^{31}P, and ^{19}F (for fluorine-containing compounds) NMR spectra of **1a**−**i**[PF_6], **3a,b**[PF_6], and some related known Fe(III) complexes, before (iii) deriving the proton and fluorine hyperfine coupling constants as well as (iv) the spin densities on selected carbon atoms of the aryl ring of these compounds. (v) The temperature dependence and (vi) the half-widths of the various signals will also be briefly examined, before (vii) deriving the self-exchange rates for selected complexes using line-broadening studies. Finally, (viii) the spin delocalization taking place in these Fe(III) acetylide compounds will be analyzed on more theoretical grounds with the help of DFT calculations.

Results

Synthesis and Characterization of the New Complexes 3a-[PF_6] and 3b[PF_6]. The known cationic Fe(III) complexes **1a**−**j**[PF_6] and **2**[PF_6] were obtained as previously described.[14,22,27] The new Fe(III) complexes ***m*-1d**[PF_6], **3a**[PF_6], and **3b**[PF_6] were isolated in a similar way from the Fe(II) parents ***m*-1d**, **3a**, and **3b** by oxidation using ferricinium hexafluorophosphate. The new Fe(II) acetylides **3a** and **3b** were themselves obtained from the Fe(II) chloride complex **2** and the preformed terminal alkynes **6a**,**b** via the vinylidene complexes **7a,b**[PF_6] using classical syntheses (Scheme 1). All the new Fe(II) and Fe(III) complexes were fully characterized and presented the expected spectroscopic features (Experimental Section).

We report in Figure 1 (a and b) the solid-state structures of **1c**[PF_6] and ***m*-1d**[PF_6], which were obtained by slow diffusion of *n*-pentane in a CH_2Cl_2 solution of the corresponding complexes. The former is a known compound that was fully characterized previously,[15] while ***m*-1d**[PF_6] is the meta-analogue of the known **1d**[PF_6].[28] There is nothing exceptional about distances and angles or the packing of these two complexes, but accurate geometrical parameters were needed for NMR calculations (see hereafter). The structures of the complexes **3a**, **3b**, and **3b**[PF_6] in the solid state were also confirmed by X-rays (Figure 1, parts c and d). The packing in the solid state as well as bond distances and angles are usual for these Fe(II) and Fe(III) arylacetylide complexes (Experimental Section), except perhaps for the torsion angle in the range 120−140° adopted by the phenyl plane with respect to the metal−C_5Me_5 axis in **3a**, **3a**[PF_6], and **3b**[PF_6].[12,14,15,28] Indeed, angles closer to 90° were most often observed in related Fe(II) and Fe(III) complexes.[12,15] In line with the additional steric bulk induced by the methyl groups on the arylalkynyl ligands, these conformations allow minimizing the intramolecular repulsive interactions with the dppe−aryl groups and the C_5Me_5−methyl groups in the solid state. In contrast, the strong bending of the C37−C38−C39 axis (171.9°) observed in **3a** cannot originate from intramolecular interactions, since such a feature is not observed for **3b**, presenting an even more hindered phenylalkynyl ligand. It certainly finds its origin in packing forces, as already observed for related compounds.[12,14]

Assignment of the ^{1}H NMR Spectra. The NMR spectra of the various samples have been recorded in either dichloromethane-d_2 or deuterated chloroform. While similar results were obtained in both solvents, the former was usually preferred for most investigations, since a slow reaction of the Fe(III) complexes was observed in the latter,[15] presumably generating the corresponding vinylidene complexes by hydrogen atom abstraction,[10f,11] even under strict absence of oxygen.[29]

In this study, the known chloride complex **2**[PF_6] was used as a benchmark for identifying the signals pertaining to the "(η^2-dppe)(η^5-C_5Me_5)Fe" core. We therefore started our investigation by monitoring the shifts of various mixtures of Fe(II) and Fe(III) redox congeners with **1a**/**1a**[PF_6], **1g**/**1g**[PF_6], and **2**/**2**[PF_6]. For all these compounds, the electron self-exchange reaction proved to be much faster than the ^{1}H NMR time scale under the measurement conditions used (see below), and an

(20) (a) Kheradmandan, S.; Venkatesan, K.; Blacque, O.; Schmalle, H.; Berke, H. *Chem.*−*Eur. J.* **2004**, *10*, 4872−4885. (b) Fernandez, F. J.; Blacque, O.; Alfonso, M.; Berke, H. *Chem. Commun.* **2001**, 1266−1267.
(21) Weyland, T.; Costuas, K.; Mari, A.; Halet, J.-F.; Lapinte, C. *Organometallics* **1998**, *17*, 5569−5579.
(22) Roger, C.; Hamon, P.; Toupet, L.; Rabaâ, H.; Saillard, J.-Y.; Hamon, J.-R.; Lapinte, C. *Organometallics* **1991**, *10*, 1045−1054.
(23) Köhler, F. H.; Prössdorf, W.; Schubert, U. *Inorg. Chem.* **1981**, *20*, 4096−4101.
(24) (a) Venkatesan, K.; Fox, T.; Schmalle, H. W.; Berke, H. *Organometallics* **2005**, *24*, 2834−2847. (b) Krivyk, V. V.; Eremenko, I. L.; Veghini, D.; Petrunenko, I. A.; Poutney, D. L.; Unseld, D.; Berke, H. *J. Organomet. Chem.* **1996**, *511*, 111−114.
(25) Balch, A. L.; Latos-Grazynski, L.; Noll, B. C.; Philips, S. L. *Inorg. Chem.* **1993**, *32*, 1124−1129.
(26) Köhler, F. H.; Hofmann, P.; Prössdorf, W. *J. Am. Chem. Soc.* **1981**, *103*, 6359−6372.
(27) Tilset, M.; Fjeldahl, I.; Hamon, J.-R.; Hamon, P.; Toupet, L.; Saillard, J.-Y.; Costuas, K.; Haynes, A. *J. Am. Chem. Soc.* **2001**, *123*, 9984−10000.
(28) Courmarcel, J.; Le Gland, G.; Toupet, L.; Paul, F.; Lapinte, C. *J. Organomet. Chem.* **2003**, *670*, 108−122.
(29) Paul, F.; Toupet, L.; Roisnel, T.; Hamon, P.; Lapinte, C. *C. R. Chim.* **2005**, *8*, 1174−1185.

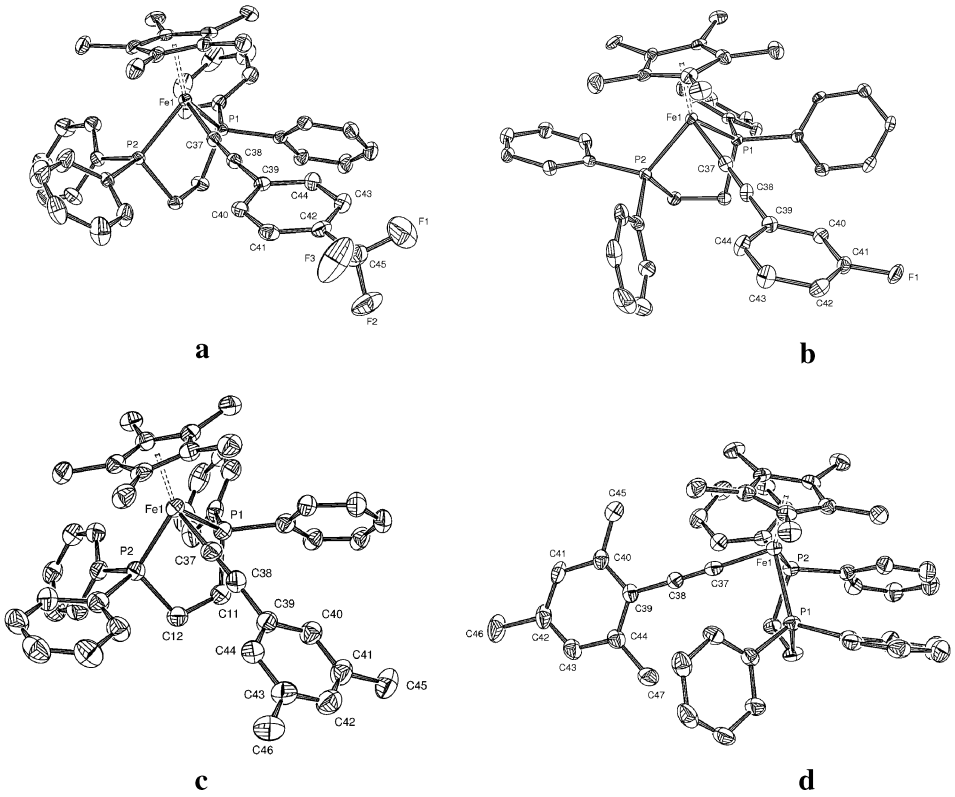

Figure 1. ORTEP representations of the cation of **1c**[PF_6] (a), the cation of ***m*-1d**[PF_6] (b), the compound **3a** (c), and the cation of **3b**[PF_6] (d) at the 50% probability level.

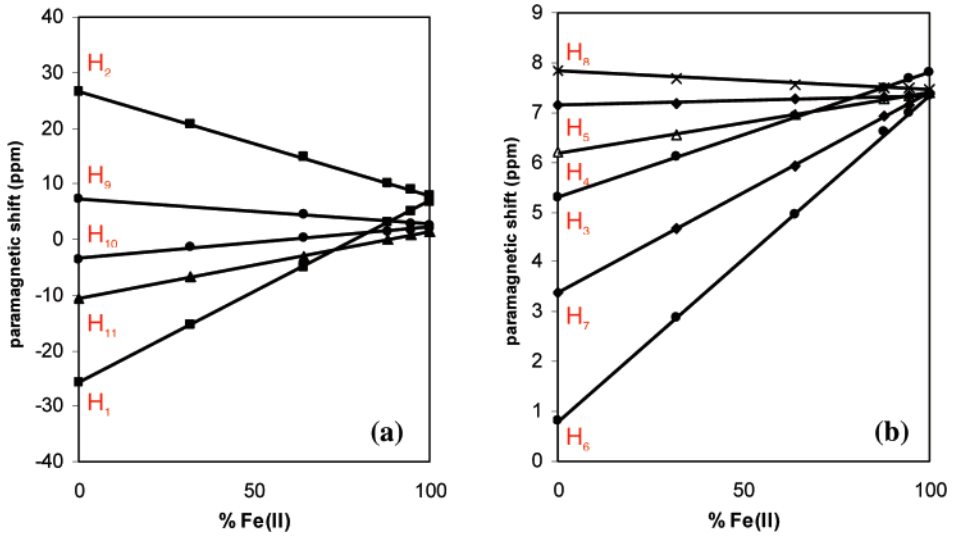

Figure 2. Observed ^{1}H NMR shifts for **1a**/**1a**[PF_6] mixtures in CD_2Cl_2 at 25 °C (assignment according to Chart 2). Aromatic protons of the dppe ligand are shown on the diagram at the right (b). For all fits $R^2 > 0.99$.

averaged single set of signals was always obtained.[22] Progressive increase in the Fe(III) concentration allowed identifying most of the signals detected for the paramagnetic complexes as shown with **1a**[PF_6] in CD_2Cl_2 (Figure 2). Similar diagrams obtained for the para-tolyl alkynyl complex **1g**[PF_6] in CD_2Cl_2 and for the chloride complex **2**[PF_6] in $CDCl_3$ are provided as Supporting Information. From these Fe(II)/Fe(III) correlations, complemented by a combination of COSY and NOESY experiments on both the diamagnetic Fe(II) and paramagnetic Fe(III) compounds **1a**−**k**/**1a**−**k**$^+$ and **3a,b**/**3a,b**$^+$, a definitive assignment (Table 1) could be gained for all the protons of the various complexes (Supporting Information). As an example, the typical spectrum of **1a**[PF_6] is shown in Figure 3, along with the corresponding assignment of the protons (Chart 2).

In all compounds, rather specific shifts were observed for the "(η^2-dppe)(η^5-C_5Me_5)Fe" core, identifying the peaks belonging to H_1 and H_2 in a straightforward way (Figure 3). These signals are usually the most upfield- and downfield-shifted peaks on the spectra of the various compounds. For **3a**[PF_6] and **3b**[PF_6], which both present methyl groups in place of these hydrogen atoms (Chart 1), the low-field and high-field signals are respectively lacking, confirming that the former signal corresponds to the meta hydrogen atoms of the arylacetylide ligand, while the latter corresponds to the ortho ones. In addition, new signals were detected at high field (−13.3 ppm) for the meta methyl groups of **3a**[PF_6] and at low field (47.4 ppm) for the ortho methyl groups for **3b**[PF_6]. The para hydrogen of the arylacetylide ligand of **3a**[PF_6] is detected at high field (−46.5

Table 1. ^{1}H NMR Shifts (δ ±0.1 ppm) Recorded for the [(η^2-dppe)(η^5-C_5Me_5)FeR][PF_6] Complexes at 20 °C in CD_2Cl_2[a]

compd	−C≡C−4−(C_6H_4)−		dppe						C_5Me_5			X
R	H_1	H_2	H_3	H_4	H_5	H_6	H_7	H_8	H_9	H_{10}	H_{11}	H_X
Cl (**2**$^+$)			7.6	6.8	6.3	2.9	4.0	7.9	11.4	−3.8	−28.3	
C≡C(C_6H_4)NO_2 (**1a**$^+$)	−25.8	26.6	5.3	7.2[b]	6.2	0.8	3.4	7.8	7.2[b,c]	−3.1	−10.7	
C≡C(C_6H_4)CN (**1b**$^+$)	−29.0	26.7	5.5	7.0	6.2	1.0	3.4	7.8	7.4[b,c]	−3.0	−10.7	
C≡C(C_6H_4)CF_3 (**1c**$^+$)	−31.2	26.8	5.9	7.0	6.2	1.2	3.5	7.8	7.7[b,c]	−2.8	−10.7	
C≡C(C_6H_4)Br (**1e**$^+$)	−40.2	29.0	6.6	6.8	6.2	1.5	3.6	7.9	n.o.[d]	−2.8	−10.5	
C≡C(C_6H_4)F (**1d**$^+$)	−43.8	27.7	n.o.[d]	6.8	6.2	1.8	3.7	7.9	n.o.[d]	−2.9	−10.5	
C≡C(C_6H_5) (**1f**$^+$)	−41.7	29.2	n.o.[d]	6.8	6.2	1.8	3.7	7.9	n.o.[d]	−2.8	−10.5	−41.7 (H_p)[b,c]
C≡C(C_6H_4)CH_3 (**1g**$^+$)	−48.2	30.0	7.4[b,c]	6.7	6.3	2.2	3.8	7.9	n.o.[d]	−3.0	−10.4	69.3 (*p*-Me)
C≡C(C_6H_4)OCH_3 (**1h**$^+$)	−55.3	26.9	8.2[b,c]	6.7	6.4	2.7	3.9	8.0	n.o[d]	−3.4	−10.2	15.3 (*p*-OMe)
C≡C(C_6H_4)NH_2 (**1i**$^+$)	−66.2	21.4	9.8[b]	6.6	6.8	3.6[b]	4.2	8.1[b]	n.o[d]	−4.5	−9.7	−3.8 (NH)[b]
C≡C(C_6H_4)NMe_2 (**1j**$^+$)	−67.4	10.0[b]	10.7[b]	6.5	7.0	4.2[b,c]	4.4	8.2	n.o.[d]	−5.1	−9.4	78.9[b]
C≡C-3,5-Xyl (**3a**$^+$)	−44.4		n.o.[d]	6.8	6.3	2.0	3.7	7.9	n.o.[d]	−2.9	−10.3	−13.3 (*m*-Me)
												−46.5 (H_p)
C≡C-2,4,6-Mes (**3b**$^+$)		33.7	7.6	6.3	6.7	2.7	4.0	8.1	n.o.[d]	−3.4	−10.5	76.9 (*p*-Me)
												47.4 (*o*-Me)
C≡C(C_6H_5)Ph (**4**$^+$)	−44.8	30.9	n.o.[d]	6.8	6.3	1.6	3.7	8.0	n.o.[d]	−2.8	−10.3	11.0 (H_m)
												−0.4 (H_o)
												−0.8 (H_p)
C≡C−3-(C_6H_4F)	−34.1	26.1	n.o.[d]	6.9	6.2	1.4	3.6	7.9	7.4[a,b]	−2.7	−10.5	−37.0 (*p*-H)
(***m*-1d**$^+$)	−34.7											

[a] Proposed assignment according to Chart 2 ($CHDCl_2$ at 5.35 ppm). [b] Tentative assignment. [c] Partly hidden behind other signals. [d] Not observed.

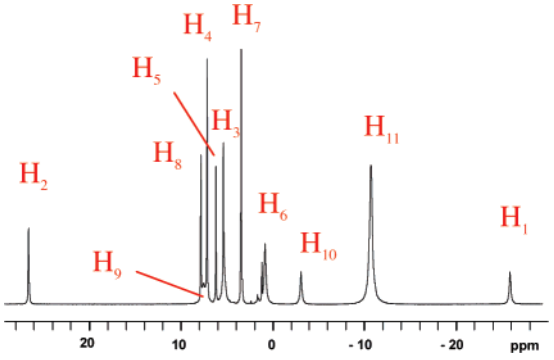

Figure 3. ^{1}H NMR spectrum of **1a**[PF_6] in CD_2Cl_2 at 25 °C with proposed assignment according to Chart 2.

Chart 2. ^{1}H Nuclei Numbering Corresponding to the Proposed Assignment

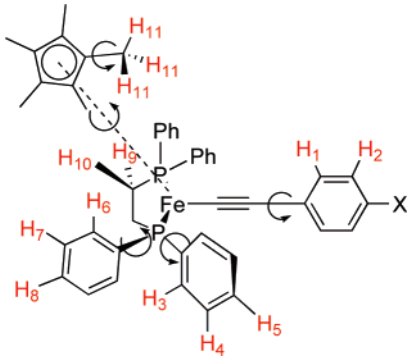

ppm), while the para methyl group of **3b**[PF_6] is strongly shifted downfield (79.9 ppm), as observed for **1g**[PF_6] (69.3 ppm). Remarkably, the signals of the ortho (H_1) and meta (H_2) ring protons appear significantly influenced by the para substituents in **1a**−**j**[PF_6]. Thus, as X becomes more electron-releasing, these peaks are more shifted and broadened. Given the increasing reactivity of compounds with electron-releasing groups, a clean spectrum of the amino-substituted complexes **1i**[PF_6] and **1j**[PF_6] proved challenging to obtain. In contrast, the most resolved spectra were obtained with compounds presenting electron-withdrawing substituents such as the nitro (**1a**[PF_6]) or the cyano (**1b**[PF_6]) complexes. The latter compounds, which

Scheme 2. Five-Membered Ring Interconversions of the $FeP_2(CH_2)_2$ Core

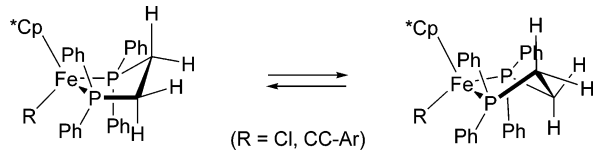

are also the least reactive in solution,[29] were therefore used for optimization of the measurement conditions.

For all Fe(III) compounds, the C_5Me_5 protons (H_{11}) correspond to the most intense peak at ca. −10 ppm. These protons exhibit the largest shifts after the protons on the arylethynyl ligand. Regarding the dppe ligand, two methylene signals are observed at 11.4 and −3.8 ppm for **2**[PF_6], which correspond to the two protons endo (near) and exo (remote) from the acetylide bond (Scheme 2). For **1a**−**j**[PF_6], the high-field dppe−methylene peak is slightly downfield shifted and observed near −3 ppm as a broad singlet. However, the second methylene signal is much more difficult to detect, since it is broader and appears at lower fields. As a result, it is usually hidden beneath more intense signals in the aromatic region. The existence of this signal, which relaxes much faster than other signals in the aromatic region, was ascertained by measurements of spin−lattice relaxation time with **1a**[PF_6] (T_1 = 2.3 ms; Supporting Information). Notably, in a frozen C_s conformation of the metalladiphosphane five-membered ring made by the chelate backbone coordinated to the iron center, each of the four methylenic protons should be distinct. However, rapid interconversions of the five-membered ring in solution result in an effective C_{2v} symmetry for the "(η^2-dppe)(η^5-C_5Me_5)Fe" core (Scheme 2), and the diagnostic AB pattern expected for the inequivalent ^{31}P nuclei in such a frozen ring is never observed by ^{31}P NMR, as can be stated with the diamagnetic Fe(II) parents **1a**−**j**.[30]

Concerning the aromatic protons of the dppe ligand, two sets of signals in a roughly 1/2/2 ratio and with increasing linewidths are observed. These can be readily assigned to para, meta, and

(30) Internal motions can be quite rapid, since variable-temperature NMR experiments on **1a**, **1g**, and **3b** revealed that no specific conformation could be frozen in solution with these compounds at temperatures down to 190 K.

Chart 3

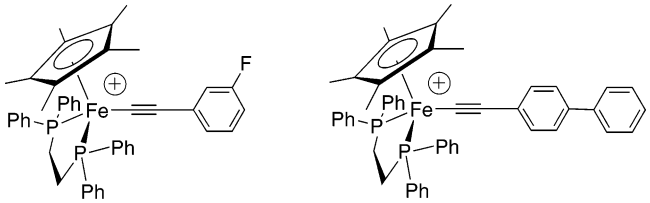

***m*-1d$^+$** **4$^+$**

ortho protons, respectively (Supporting Information), the latter being possibly in part broadened by unresolved coupling to phosphorus. Similar to the methylenic dppe signals H_9 and H_{10}, these two sets correspond to phenyl rings "close" (endo) and "remote" (exo) from the acetylide bond, respectively (Chart 2). Notably, the peaks attributed to the phenyl protons H_3, H_4, and H_5 and to the methylene proton H_9 correspond to the most broadened, but also to the least shifted signals among those of the dppe aromatic protons.

We next recorded the ^{1}H NMR spectra of ***m*-1d**[PF_6] and of the known **4**[PF_6][10a] complexes (Chart 3). For the former complex, some uncertainty remains regarding the assignment of the ortho and para protons on the fluorinated aryl ring, both signals being shifted to high fields (Table 1). We propose that the two signals at high field near −34 ppm correspond to the two nonequivalent ortho protons, while the more shifted signal near −37 ppm would correspond to the para proton. The nonequivalence of the two ortho protons must be weak, because the corresponding carbon atoms are also not differentiated in the ^{13}C NMR (see below). For **4**[PF_6], all the new peaks can be attributed on the basis of their integrations and shifts (Table 1).

Assignment of the ^{13}C NMR Spectra. The ^{13}C NMR spectra of all the Fe(III) compounds were next recorded. As for the ^{1}H NMR spectra, we started by monitoring the shifts of mixtures of **1a** and **1a**[PF_6] in order to assign the various signals detected (Figure 4). Owing to the rapid self-exchange reaction, an averaged set of peaks was always obtained for the various mixtures tested. All observed signals could be identified. Thus, the peaks corresponding to the two ipso carbon atoms of the dppe aromatic rings (C_7 and C_{11}) and to the α-carbon of the alkynyl ligand (C_1) are lacking, while the peaks of all other carbon atoms were detected in the 900/−200 ppm range. These signals have already disappeared when only 5% of Fe(III) has been added to the solution of corresponding Fe(II) complex. More generally, with **1a**−**j**[PF_6] we were unable to detect any peaks outside this spectral range, even up to 4000 ppm and down to −1000 ppm. Given the similarities between spectra, assignments similar to those of **1a**[PF_6] were taken for other compounds (Table 2). The typical ^{13}C NMR spectrum of **1a**[PF_6] is shown in Figure 5, along with the corresponding assignment of the carbon nuclei (Chart 4).

Again, a quite specific signature is observed for the "(η^2-dppe)(η^5-C_5Me_5)Fe" core, which is exemplified by the ^{13}C NMR spectrum of **2**[PF_6]. Depending on the complex considered, the singlet corresponding to the methyl groups of the C_5Me_5 ligand (C_{17}) is shifted downfield (**2**[PF_6]) or upfield (other compounds) in comparison to its position in the corresponding Fe(II) complex, while the peak of the inner carbon atoms of the cyclopentadienyl ligand (C_{16}) is always shifted to low field. The latter is detected at 223.3 ppm for **2**[PF_6] and lies around 175 ppm for **1a**−**j**[PF_6] (Table 2). Regarding the dppe ligand, the signals of the quaternary ipso carbons of the two nonequivalents phenyl rings of the dppe ligand were not detected, while those corresponding to the various primary carbon nuclei are clustered in the 120−160 ppm region. Their exact assignment was subsequently obtained from the ^{1}H assignment with the help of HMQC correlations (Table 2). As already observed in the ^{1}H NMR spectra, the peaks of the ortho carbon nuclei are significantly broader than those of the meta and para carbon atoms. In the ^{13}C NMR spectra, these signals are also more shifted than those of the meta and para carbon atoms. Notably, the peak corresponding to the methylene carbon atoms of the dppe, observed near −190 ppm in all compounds, is not detected with **2**[PF_6].[31]

Regarding the arylethynyl carbon nuclei, the signals of the acetylide α-carbon atoms (C_1) escaped detection for the Fe(III) acetylide complexes presently investigated (Figure 4), in contrast to the peaks of the β-carbon atoms (C_2), which were most often detected. These signals constitute the most downfield-shifted peaks of the various ^{13}C NMR spectra (Figure 5). In this connection, the most upfield-shifted peaks among the signals detected for the arylethynyl ligands in **1a**−**h**[PF_6] correspond to the nearby carbon atom (C_3), in para-position to the X-substituent. These very diagnostic peaks become broader for the Fe(III) compounds with more electron-releasing substituents and eventually become undetectable in **1i**[PF_6] and **1j**[PF_6]. As already observed on the ^{1}H NMR spectra, the ^{13}C NMR chemical shifts of the arylethynyl ligand are quite substituent-sensitive for **1a**−**i**[PF_6] and are overall larger than those undergone by the carbon nuclei on other ligands.

The ^{13}C NMR spectra of the ***m*-1d**[PF_6] and **4**[PF_6] complexes were next assigned on the basis of these results and of the relative intensity of the detected signals (Table 2). For the former compound, only one additional peak relative to **1d**[PF_6] was detected. The unique singlet appearing at high field certainly corresponds to the overlapping signals of the two chemically nonequivalent ortho *C*-H carbon nuclei of the fluorinated aryl ring, while the *C*-H meta carbon nucleus is observed as expected, near −33 ppm. The *C*-F meta carbon atom is observed near 20 ppm, as a poorly resolved multiplet with a doublet-like shape ($^1J_{CF}$ of ca. 240 Hz in ***m*-1d**).[28] For **4**[PF_6], three additional signals were detected relative to **1f**[PF_6]. Two of these, near 200 ppm, correspond to the ortho and para *C*-H carbon nuclei of the phenyl substituent. As expected from their more remote position from the metal center, they are less shifted than the peaks corresponding to C_4 and C_6 (Chart 4). The remaining new peak near −12 ppm is tentatively attributed to the ipso carbon atom. The missing peak that corresponds to the two meta *C*-H carbons is possibly hidden behind the ortho dppe signal near 96 ppm (C_{12}).

^{31}P NMR Spectra. So far, ^{31}P NMR signals have never been detected between 500 and −500 ppm for all the Fe(III) complexes of this kind ever investigated.[6a] To make sure about the possibility to detect this signal, we have decided to monitor the shift of the phosphorus atom using various **1a**/**1a**[PF_6] mixtures. Thus, we started from pure **1a** (δ_P = 100.6 ppm) and progressively increased the amount of **1a**[PF_6] in the solution (Figure 6). The sharp phosphorus signal of **1a** near 100 ppm readily broadened and was strongly shifted toward high fields already when traces of **1a**[PF_6] complex were admixed. Above 10%, the signal rapidly flattened and eventually disappeared in the baseline, possibly because of the increasing contribution of line-broadening effects due to the electron self-exchange process (vide infra). By extrapolation, we could infer that the ^{31}P NMR

(31) For **2**[PF_6] qualitatively similar spectra featuring the same number of peaks were observed in DMSO-d_6 when the temperature of the sample was varied from 25 to 50 °C (above this temperature, **2**[PF_6] decomposes), rendering any coincidental overlap of the missing ipso carbon and methylene signals unlikely.

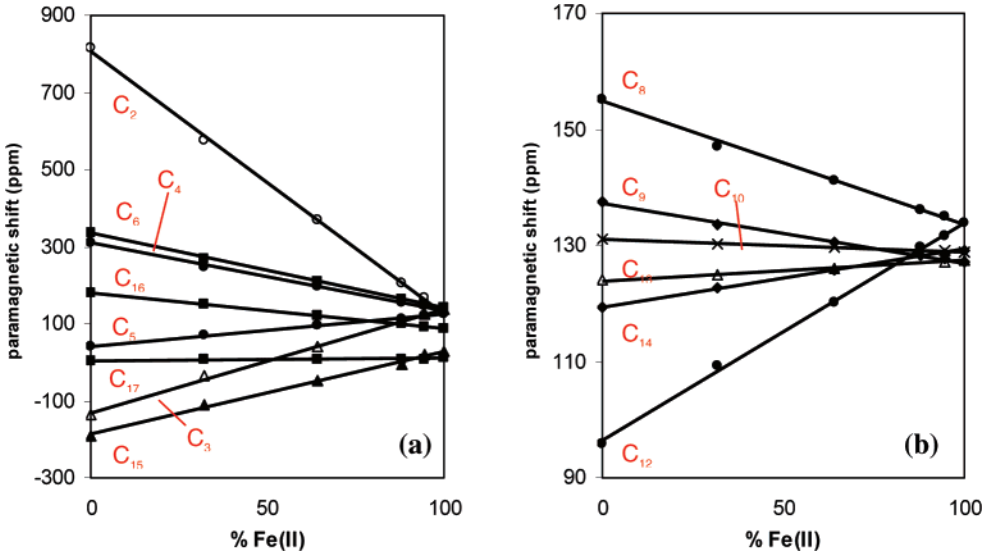

Figure 4. Observed ^{13}C NMR shifts for **1a**/**1a**[PF_6] mixtures in CD_2Cl_2 at 25 °C (assignment according to Chart 4). Aromatic carbon nuclei of the dppe ligand are shown on the diagram at the right (b). For all fits $R^2 > 0.99$.

Table 2. ^{13}C NMR Shifts (δ ±0.1 ppm) recorded for Selected [(η^2-dppe)(η^5-C_5Me_5)FeR][PF_6] Complexes at 20 °C in CD_2Cl_2[a]

compd	C≡C−4−(C_6H_4)−					dppe							C_5Me_5		X
R	C_2	C_3	C_4	C_5	C_6	C_8	C_9	C_{10}	C_{12}	C_{13}	C_{14}	C_{15}	C_{16}	C_{17}	C_X
Cl (**2**$^+$)						159.0	134.5	131.2	98.9	123.9	121.0	n.o.[b]	223.3	22.2	
C≡C(C_6H_4)NO_2 (**1a**$^+$)	817.5	−134.0	311.2	40.0	336.6	155.3	137.5	131.2	95.8	124.0	119.4	−188.7	181.7	3.6	
C≡C(C_6H_4)CN (**1b**$^+$)	789.5	−130.7	299.2	32.0	307.2	154.5	136.9	131.0	96.3	123.8	119.8	−184.6	179.4	2.7	−16.0
C≡C(C_6H_4)CF_3 (**1c**$^+$)	791.3	−134.7	292.3	12.4	332.9	154.8	136.6	130.6	95.8	123.6	119.8	−186.1	177.9	1.6	30.4[c]
C≡C(C_6H_4)Br (**1e**$^+$)	762.7	−143.0	276.3	−45.9	455.4	154.4	136.3	132.1	95.6	123.1	120.0	−188.3	174.5	−0.5	
C≡C(C_6H_4)F (**1d**$^+$)	744.5	−146.9	267.8	−84.6	467.9	154.5	136.2	129.5	95.5	122.7	120.1	−189.1	173.2	−2.1	
C≡C(C_6H_5) (**1f**$^+$)	774.4	−147.0	267.0	−50.8	396.2	155.0	135.7	130.8	95.2	122.5	119.7	−189.1	173.0	−2.2	
C≡C(C_6H_4)CH_3 (**1g**$^+$)	748.8	−152.4	255.2	−101.0	475.7	155.5	136.1	129.2	95.9	122.5	120.4	−189.5	170.7	−3.2	−112.5[c]
C≡C(C_6H_4)OCH_3 (**1h**$^+$)	707.8	−158.7	239.8	−151.9	497.3	155.4	136.2	128.4	96.5	122.1	120.6	−189.3	167.8	−4.7	n.o.[b,d]
C≡C(C_6H_4)NH_2 (**1i**$^+$)	n.o.[b]	n.o.[b]	206.4	n.o.[b]	n.o.[b]	157.7	137.2	129.2	96.8	121.6	121.6	−187.9	161.0	−7.3	
C≡C(C_6H_4)NMe_2 (**1j**$^+$)	n.o.[b]	n.o.[b]	n.o.[b]	n.o.[b]	n.o.[b]	158.9	137.9	129.1	101.4	121.4	122.4	−189.9	158.9	−9.0	−81.7[c]
C≡C−3,5-Xyl (**3a**$^+$)	767.3	−150.4	258.4	−66.2	429.7	155.6	135.8	129.3	95.6	122.4	119.8	−189.7	171.2	−3.2	61.9
C≡C−2,4,6-Mes (**3b**$^+$)	776.4	−160.1	239.0	−127.8	552.3	158.2	136.6	129.6	96.3	121.6	121.0	−198.7	163.5	−3.5	−82.7 −160.0[c]
C≡C(C_6H_5)Ph (**4**$^+$)	760.0	−149.1	263.8	−88.1	461.3	155.1	136.0	129.3	95.8	122.6	120.1	−188.8	172.3	−2.4	231.0[e] 174.1[f] n.o.[g] −12.2[h]
C≡C−3-(C_6H_4F) (***m*-1d**$^+$)	758.6	−139.6	281.1[i]	−32.9	345.8	154.2	135.8	129.8	95.3	122.8	119.5	−187.1	175.0	−0.2	18.0[j]

[a] Proposed attribution according to Chart 4 (CD_2Cl_2 at 53.8 ppm). [b] Not observed. [c] Tentative assignment (broad and weak signal). [d] Possibly hidden beneath another signal. [e] Ortho carbon atoms. [f] Para carbon atom. [g] Meta carbon atoms. [h] Ipso carbon atom. [i] Inequivalent ortho carbon atoms apparently not differentiated by meta-substitution. [j] Functional meta carbon (C−F).

signal for neat **1a**$^+$ should lie around −3000 ppm. Actually, this signal was detected as a broad singlet ($\nu_{1/2}$ of ca. 13 000 Hz) with a pure sample of **1a**[PF_6], due to the absence of self-exchange. However, due to the very bad baseline obtained for such a large spectral window with our probe, phasing of the spectra proved problematic and a large uncertainty certainly exists for the shift of this signal. Related ^{31}P NMR signals were also detected around 3000 ± 300 ppm for **1f**[PF_6], **1h**[PF_6], **1i**[PF_6], and **2**[PF_6]. These shifts should however be considered with caution in the absence of extrapolated estimates from corresponding Fe(III)/Fe(II) correlations.

^{19}F NMR Spectra. For the complexes **1c**[PF_6], **1d**[PF_6], and ***m*-1d**[PF_6] in CD_2Cl_2, broad ^{19}F NMR signals could be detected in the usual ^{19}F NMR range (Table 3). Thus, in addition to the expected doublet of the PF_6^- counterion near −74 ppm ($^1J_{PF}$ of ca. 710 Hz), a broad singlet ($\nu_{1/2}$ = 200 Hz) was observed at −15.1 ppm for **1c**[PF_6], i.e., downfield to the signal previously reported for **1c** at −61.5 ppm in $CDCl_3$.[14] For **1d**[PF_6] a very broad singlet ($\nu_{1/2}$ = 2500 Hz) was observed at 13.3 ppm in CD_2Cl_2, i.e., also downfield to the ^{19}F NMR peak of the Fe(II) parent (−119.8 ppm), while for ***m*-1d**[PF_6], a comparably narrower ($\nu_{1/2}$ = 160 Hz) singlet was detected at −137.4 ppm, this time upfield to the signal of ***m*-1d** (−115.8 ppm).[28]

Derivation of Selected Hyperfine Coupling Constants. As shown in eq 1, the observed paramagnetic shift of a given nucleus is the sum of a diamagnetic contribution (δ_{dia}), which

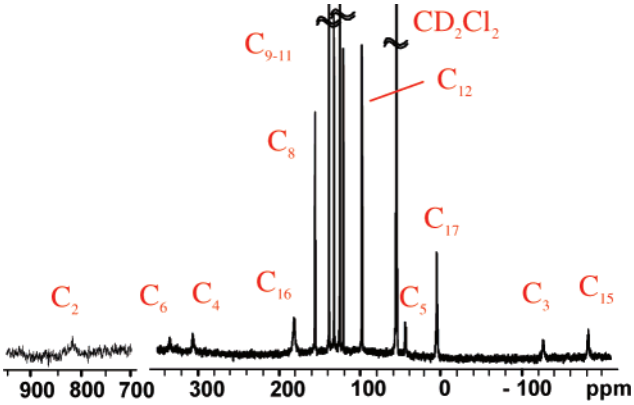

Figure 5. ^{13}C NMR spectrum of **1a**[PF_6] in CD_2Cl_2 at 25 °C with proposed assignment according to Chart 4. The two parts correspond to two spectra with different offsets (intensities are arbitrary).

Chart 4. ^{13}C Nuclei Numbering Corresponding to the Proposed Assignment

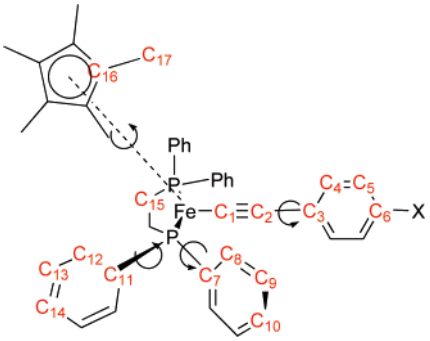

corresponds to the shift that the compound would present without any unpaired electron, and the isotropic contribution (δ_{iso}), which precisely represents the additional contribution to the shift due to the presence of the unpaired electron(s) in the compound.[17] For the Fe(III) complexes under investigation, the former contribution (δ_{dia}) can be approximated by the shift of the nucleus considered in the diamagnetic Fe(II) parent.

$$\delta_{obs} = \delta_{dia} + \delta_{iso} \quad (1)$$

The remaining isotropic shift (δ_{iso}) can also be split into two contributions, called contact (δ_c) and pseudocontact (δ_{pc}) shifts (eq 2a).[17] The pseudocontact (or dipolar) shift (δ_{pc}) results from the through-space dipolar interaction between the nuclear spin and the unpaired electron, while the contact contribution (δ_c) results from Fermi coupling (through-bond interaction) between the nuclear spin and the unpaired electron. This shift is directly proportional to the local spin density in s-type atomic orbitals (AOs) and allows derivation of the corresponding hyperfine coupling constant, as defined for organic radicals. However, in order to access the desired hyperfine coupling constant from the isotropic shift, the pseudocontact contribution originating from metal center $(\delta_{pc})^M$ needs to be reliably estimated first.

$$\delta_{iso} = \delta_c + \delta_{pc} \quad (2a)$$

$$\delta_{pc} = (\delta_{pc})^M + (\delta_{pc})^L \quad (2b)$$

As shown in eq 2b, the pseudocontact shift can itself be decomposed into two contributions. In complexes where the unpaired electron mostly resides on the metal center, the ligand-centered term $(\delta_{pc})^L$ is usually neglected for hydrogen nuclei. Most often, the pseudocontact shift is therefore considered to

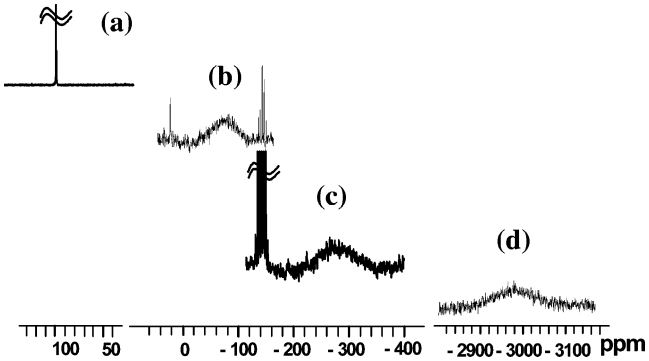

Figure 6. ^{31}P NMR spectra of **1a/1a**[PF_6] mixtures at 25 °C in CD_2Cl_2 for 0% (a), 5% (b), 12% (c), and 100% (d) of Fe(III) complex (intensities are arbitrary). The signal of the PF_6^- counterion can also be observed near −140 ppm. The observed line-broadening of the signal upon increasing concentrations of Fe(II) complex matches with that expected for the self-exchange reaction under fast exchange conditions.

Table 3. ^{19}F NMR Shifts, Half-widths, Isotropic Shifts, Estimated Isotropic Hyperfine Coupling Constants (G), and Computed Pseudocontact Shifts (ppm) for Selected [(η^2-dppe)(η^5-C_5Me_5)FeC≡C−Ar_F][PF_6] Complexes at 20 °C in CD_2Cl_2 at 500 MHz

compd Ar_F	δ^a (ppm)	$\nu_{1/2}$ (Hz)	$\delta_{iso}{}^a$ (ppm)	$a_F{}^b$ (G)	$(\delta_{pc})^{M\ a,c}$ (ppm)
4-$C_4H_4(CF_3)$	−15.1	200[d]	46.4	0.49	1.0
4-C_4H_4F	13.5	2500[e]	133.5	1.44	1.0
3-C_4H_4F	−137.5	160[d]	−20.5	−0.23	1.3

[a] ±0.5 ppm. [b]Estimates obtained from eq 4. [c]Obtained from eq 3. [d]±10 Hz. [e]±100 Hz.

result solely from the metal-centered term $(\delta_{pc})^M$. This contribution can be computed from the geometric parameters of the complex, provided the magnetic anisotropy or the diagonal values of the *g*-tensor are known. Thus, for **1a**−**j**[PF_6], a rhombic anisotropy should have been considered based on ESR data.[15] However, considering (i) the very fluxional nature of these complexes in solution (see Scheme 2 for instance), (ii) the very facile rotation of the arylacetylide ligand around its axis (see later), and (iii) the uncertainties regarding the precise orientation of the *g*-tensor along with the overall weak rhombicity of the *g*-tensor ($g_3 > g_2 \approx g_e \approx g_1$),[32] we have chosen to simplify the derivation of $(\delta_{pc})^M$ by considering an axial anisotropy instead. Thus, we have used eq 3[17] with $g_{||} = g_3$ directed along the acetylide axis and $g_\perp = (g_2 + g_1)/2$ to compute the pseudocontact shifts for protons of the arylacetylide ligand in which we were primarily interested (Table 4).[33] As can be seen from the values found, the metal-centered pseudocontact contribution to the shifts of these protons is quite weak in **1a**−**j**[PF_6] or **3a,b**[PF_6], since the estimates obtained fol-

(32) Analysis of the frontier molecular orbitals (MOs) in a previous DFT study conducted on computationally simpler model compounds suggested that the direction of the strongest diagonal component ($g_{zz} = g_3$) was roughly along the acetylide axis in **1a**−**j**[PF_6], but slight deviations were predicted to take place, especially with strongly electron-withdrawing substituents.[15]

(33) In this expression, r_M is the distance from the metal center to the nuclei, θ is the corresponding angle with the acetylide axis, and the symbols have their usual meaning.[34] The geometric parameters (r_M and θ) were obtained from the corresponding X-ray structures after averaging the data for equivalent nuclei in solution. The δ_{pc} values computed for several complexes are given in Table 4. Notably, eq 3 is reliable for r_M values larger than 4 Å (less than 10% accurate if not).[35,40] Thus, δ_{pc} values derived by this equation should be considered with care for nuclei closer to the metal center or for nuclei on very fluxional ligands (due to the inherent imprecision on the geometric factors). This is, however, not the case for the detected nuclei of the arylacetylide ligand.

Table 4. Experimental Paramagnetic Shifts (δ (ppm) $\pm$ 0.1), Calculated Metal-Centered Pseudocontact Shifts (δ_{pc}), and Resultant Contact Shifts (δ_c) for Arylacetylide Protons of Selected [(η^2-dppe)(η^5-C_5Me_5)FeC$\equiv$C$-$Ar][PF_6] Complexes at 20 °C in CD_2Cl_2 (5.35 ppm)

compd Ar		Ar H_1	Ar H_2	X H_X
$(C_6H_4)NO_2$	δ_i	-32.6	18.7	
(**1a**$^+$)	δ_{pc}[a]	3.7	1.5	
	δ_c	-36.3	17.2	
$(C_6H_4)CH_3$	δ_i	-55.0	23.1	67.1
(**1g**$^+$)	δ_{pc}[a]	3.5	1.5	0.8
	δ_c	-58.5	21.6	66.3
$(C_6H_4)NH_2$	δ_i	-73.4	15.0	-6.0
(**1i**$^+$)	δ_{pc}[a]	2.4	1.0	0.6
	δ_c	-75.8	145.0	-6.6
3,5-Xyl	δ_i	-51.4	-15.5[b]	-53.5[c]
(**3a**$^+$)	δ_{pc}[a]	3.4	0.6[b]	1.1[c]
	δ_c	-54.8	-16.1[b]	-54.6[c]
2,4,6-Mes	δ_i	45.3[d]	26.4	74.7[e]
(**3b**$^+$)	δ_{pc}[a]	2.5[d]	1.4	0.8[e]
	δ_c	42.8[d]	25.0	73.9[e]

[a] Computed from eq 3 and crystallographic data. [b] Methyl group in meta position. [c] Proton in para position. [d] Methyl group in ortho position. [e] Methyl group in para position.

lowing our approximation remain below 7% of the isotropic shifts, except for the meta protons of **1a**[PF_6], where they amount to 12% of the isotropic shift. In regard to the relative weakness of this contribution, eq 3 certainly constitutes a convenient and straightforward means to get a fair estimate of the pseudocontact shifts (δ_{pc}) for H_1 and H_2 in these compounds and provides thereby an access to the corresponding contact contributions (δ_c) via eq 2a.

$$(\delta_{pc})^M = (\mu_0/4\pi)(\mu_B{}^2/9kT)[S(S+1)](g_{\parallel}{}^2 - g_{\perp}{}^2)(3\cos^2\theta - 1)/r_M{}^3 \quad (3)$$

From the contact shifts, the hyperfine coupling constants between the unpaired electron and the protons considered were obtained using eq 4 (N = H).[17] In this expression, g represents the isotropic g value, S is its spin quantum number, T is the temperature in Kelvin, while other symbols have their usual meaning.[34] The isotropic g values needed in eq 4 were obtained by averaging the three diagonal g values experimentally determined at low temperature by ESR for the various Fe(III) complexes.[15] The values found for hydrogen and fluorine atoms of the arylacetylide ligands in **1a**$-$**j**[PF_6], ***m*-1d**[PF_6], **3a,b**[PF_6], and **4**[PF_6] are given in Tables 3 and 5. Given the approximations made, these figures are evidently only estimates of the exact hyperfine coupling constants with these nuclei. Note however that due to the poor resolution achieved during ESR measurements on frozen glass samples, such data could not be formerly obtained.

$$a_N = \delta_c \times \hbar 3\gamma_N kT/(g\mu_B S(S+1)) \quad (4)$$

Derivation of Spin Densities on Selected Nuclei. According to McConnell, the contact contribution to ^{1}H NMR shifts of aromatic radicals is directly proportional to the local spin density

Table 5. Isotropic Hyperfine Coupling Constants (in G) with Selected Protons for [(η^2-dppe)(η^5-C_5Me_5)FeR][PF_6] Complexes

compd R = $-$C$\equiv$C$-$4-(C_6H_4)X	hyperfine constants a_{H1}	a_{H2}	a_{HX}
C$\equiv$C(C_6H_4)NO_2 (**1a**$^+$)	-0.42	0.20	
C$\equiv$C(C_6H_4)CN (**1b**$^+$)	-0.45	0.21	
C$\equiv$C(C_6H_4)CF_3 (**1c**$^+$)	-0.48	0.21	
C$\equiv$C(C_6H_4)Br (**1e**$^+$)	-0.59	0.23	
C$\equiv$C(C_6H_4)F (**1d**$^+$)	-0.63	0.22	
C$\equiv$C(C_6H_5) (**1f**$^+$)	-0.61	0.24	-0.61[a]
C$\equiv$C(C_6H_4)CH_3 (**1g**$^+$)	-0.69	0.25	0.78
C$\equiv$C(C_6H_4)OCH_3 (**1h**$^+$)	-0.78	0.23	0.13
C$\equiv$C(C_6H_4)NH_2 (**1i**$^+$)	-0.91	0.17	-0.08
C$\equiv$C(C_6H_4)NMe_2 (**1j**$^+$)	-0.93	0.04	0.93[b]
C$\equiv$C$-$3,5-Xyl (**3a**$^+$)	-0.64	-0.19 [c]	-0.64[a]
C$\equiv$C$-$2,4,6-Mes (**3b**$^+$)	0.50[d]	0.29	0.87[e]
C$\equiv$C$-$3-(C_6H_4F) (***m*-1a**$^+$)	-0.52	0.20	-0.53 [f]
	-0.53		
C$\equiv$C$-$2-(C_6H_4)-1,1′-(C_6H_2) (**4**$^+$)	-0.65	0.26	-0.10[g]
			-0.10[g]
			0.03[h]

[a] Proton in para position. [b] Methyl groups on nitrogen. [c] Methyl group in meta position. [d] Methyl group in ortho position. [e] Methyl group in para position. [f] Proton in para position. [g] Protons in ortho and para positions on the second ring. [h] Proton in meta position on the second ring.

Table 6. π-Charge (e) on the Primary Carbon Atoms of the Arylacetylide Ligand as Deduced from McConnell and Karplus & Fraenkel Equations for [(η^2-dppe)(η^5-C_5Me_5)FeR][PF_6] Complexes[37]

compd R	C$\equiv$C$-$4$-$C$_6$H$_4$X $(\rho^\pi)_{C4}$[a]	$(\rho^\pi)_{C5}$[a]	$(\rho^\pi)_{C6}$	$(\rho^\pi)_X$
C$\equiv$C(C_6H_4)NO_2	0.019	-0.009		
C$\equiv$C(C_6H_4)CN	0.021	-0.010		
C$\equiv$C(C_6H_4)CF_3	0.022	-0.010	0.014[b]	
C$\equiv$C(C_6H_4)Br	0.027	-0.011		
C$\equiv$C(C_6H_4)F	0.029	-0.010		
C$\equiv$C(C_6H_5)	0.028	-0.011	0.027	
CC(C_6H_4)CH_3	0.031	-0.012	0.031[c]	
CC(C_6H_4)OCH_3	0.035	-0.010		
C$\equiv$C(C_6H_4)NH_2	0.040	-0.007	-0.003[c]	
C$\equiv$C(C_6H_4)NMe_2	0.040	-0.002		
CC$-$3,5-Xyl	0.029	-0.008[c,d]	0.029	
C$\equiv$C$-$2,4,6-Mes	0.020[c,e]	-0.013	0.034[c,f]	
C$\equiv$C$-$3-(C_6H_4F)	0.024	-0.009	0.023	
	0.024			
C$\equiv$C$-$4-(C_6H_4)Ph	0.029	-0.012		0.004[g]
				-0.001[h]
				0.004[g]

[a] Determined from δ_C and eq 5. [b] A value of 107.6 MHz has been used for $(Q_{C-CF3})^F$ with the ^{19}F NMR isotropic shift corrected for the metal-centered dipolar contribution.[39] [c] A value of 75 MHz has been used for $(Q_{C-CH3})^H$ and for $(Q_{C-NH2})^H$. [d] Methyl group in meta position. [e] Methyl groups in ortho position. [f] Methyl group in para position. [g] Protons in ortho and para positions on the second ring. [h] Proton in meta position on the second ring.

in the p_z atomic orbital (AO) of the carbon atom bearing the hydrogen nucleus.[18,36] The latter can be deduced using the so-called McConnell equation (eq 5), where $(Q_{CH})^H$ is a constant amounting to ca. -66 MHz (Table 6).[36b,37] For methyl groups,

(34) μ_0 is the vacuum permitivity, γ_N are the magnetogyric ratio of the nuclei N, μ_B is the Bohr magneton, k is the Boltzman constant, $\hbar$ is the reduced Planck constant, g_e is the free electron g value, and N is the Avogadro number.

(35) (a) Golding, R. M.; Pascual, R. O.; Vrbancich, J. *Mol. Phys.* **1976**, *31*, 731$-$744. (b) Golding, R. M.; Pascual, R. O. *Bull. Magn. Reson.* **1983**, *5*, 126$-$128.

(36) (a) McConnell, H. M.; Chesnut, D. B. *J. Chem. Phys.* **1958**, *27*, 984$-$985. (b) McConnell, H. A. *J. Chem. Phys.* **1958**, *28*, 1188$-$1192.

(37) Karplus, M.; Fraenkel, G. K. *J. Chem. Phys.* **1961**, *35*, 1312$-$1323.

(38) Mispelter, J.; Momenteau, M.; Lhoste, J.-M. In *Biological Magnetic Resonance*; Berliner, L. J., Reuben, J., Eds.; Plenum Press: New York, 1993; Vol. 12, pp 299$-$355.

(39) Eaton, D. R.; Josey, A. D.; Sheppard, W. *J. Am. Chem. Soc.* **1963**, *85*, 2689$-$2694.

constants of 75 MHz have been used in **1g**[PF_6] and **3a,b**[PF_6].

$$(a_H)^{\pi} = (Q_{CH})^H(\rho^{\pi})_C \quad (5)$$

While the carbon spin densities obtained by these means can be considered with confidence for primary carbon atoms in complexes with electron-withdrawing substituents, the spin densities obtained for the carbons bearing electron-releasing substituents are certainly less reliable because of the neglect of the contribution of local dipolar shifts in our treatment (see below). Also, given the known variability of the corresponding Q factor, for which several values have been computed or measured depending on the compounds, the charge derived for the few quaternary carbons bearing a methyl substituent should also be considered with great care.[17]

Temperature Dependence of the ^{1}H NMR Signals. We have next examined the temperature dependence of the ^{1}H NMR shifts of **1a**[PF_6], **1g**[PF_6], and **2**[PF_6] between 297 and 183 K. For each peak, the temperature dependence of the isotropic shift (δ_{iso}) provides information about the energetic degeneracy of the ground state (GS) of the paramagnetic compound under investigation and on its separation from the first excited states.[17] As shown in eq 2a, the isotropic shift is the sum of the contact (δ_c) and pseudocontact (δ_{pc}) shifts. For paramagnetic compounds with a nondegenerate GS and high-lying excited states, the isotropic shift should exhibit a $1/T$ dependence converging toward zero for T reaching infinity (Curie behavior), since both the contact (δ_c) and the pseudocontact (δ_{pc}) contributions are expected to follow such a trend.[17,40] As shown in Figure 7 for **1g**[PF_6], linear plots were obtained against $1/T$ with overall very good fits for all signals in the temperature range investigated (Table 7). This linear dependence is clearly in line with the Curie behavior expected for these compounds. Except for the ortho protons (H_1) of the arylalkynyl ligand in **1a**[PF_6] and for the C_5Me_5 protons (H_{11}) in **2**[PF_6], the shifts of the protons in the different complexes correspond quite satisfyingly to those of the diamagnetic Fe(II) parents (δ_{dia} in eq 1) when extrapolated at infinite temperature, especially when considering the inherently large error of such a procedure (Table 7). Thus, we believe that the discrepancies observed for H_1 in **1a**[PF_6] and H_{11} in **2**[PF_6] are not indicative of a GS degeneracy, nor of closely lying excited states. We would rather tentatively propose that they result from the stabilization of some conformations, solvent adducts, or aggregates presenting less spin density on H_1 or H_{11} when the temperature is decreased.[42]

Electronic and Rotational Correlation Times Deduced from the ^{1}H NMR Signals. The half-widths ($\nu_{1/2}$) of the various NMR signals were also measured. These data are inversely proportional to the transverse relaxation rates (T_{2M}) (eq 6) and convey therefore important information about the relaxation processes operative in solution.

$$\pi(\nu_{1/2}) = (T_2^*)^{-1} \quad (6)$$

The T_2* values previously determined for the various protons in **1a**[PF_6] or **1b**[PF_6] according to eq 6 are clearly shorter than the longitudinal relaxation rates (T_1, Supporting Information). Considering $T_2 = T_2$* (i.e., neglecting any contribution to the linewidths due to the magnetic field inhomogeneity), the longer values found for T_1 in comparison to T_2* indicate that we are not in the so-called fast motion limit.[17] Consequently, the T_2 values determined for protons in **1a**−**j**[PF_6] can be approximated by eq 7a (see also Supporting Information). This expression is a sum of different terms corresponding to distinct relaxation mechanisms.[44] The first term pertains to dipolar relaxation and the second to contact relaxation.[45] In this expression, the correlation time (τ_c) of the dipolar relaxation is determined by the rotational correlation time (τ_r) and by the electronic correlation time (τ_e) according to eq 7d. Examination of the field dependence of the half-widths of the various peaks in the ^{1}H NMR spectra for **1a**[PF_6], **1g**[PF_6], and **2**[PF_6] over a 200, 300, and 500 MHz apparatus reveals a poor sensitivity to the field strength (Supporting Information). This suggests that the transverse relaxation rates are not dispersed owing to $1/(1 + \tau^2\omega_s^2)$ terms ($\tau = \tau_c$ or τ_e) and, therefore, that these terms might be neglected in the spectral density functions (eqs 7b and 7c).

$$(T_{2M})^{-1} = (1/15)(\mu_0/4\pi)^2(\gamma_H{}^2 g^2 \mu_B{}^2 S(S+1)/r_M{}^6) f_{dip}(\omega,\tau_c) + (1/3)S(S+1)(a_H/\hbar)^2 f_{con}(\omega,\tau_e) \quad (7a)$$

$$f_{dip}(\omega,\tau_c) = 7\tau_c + [13\tau_c/(1 + \tau_c{}^2\omega_s{}^2)] \quad (7b)$$

$$f_{con}(\omega,\tau_s) = \tau_e + [\tau_e/(1 + \tau_e{}^2\omega_s{}^2)] \quad (7c)$$

$$(\tau_c)^{-1} = (\tau_e)^{-1} + (\tau_r)^{-1} \quad (7d)$$

Also, it seems that no particular mechanism dominates the relaxation process of all protons in these compounds.[46] Most probably, an interplay of the dipolar and contact relaxation operates, as often observed with paramagnetic complexes. However, because of the $(r_M)^{-6}$ dependence of the metal-centered dipolar relaxation, the contact relaxation can be expected to become the dominant relaxation process for protons situated at the periphery of the compounds, provided sufficient spin density is delocalized to these nuclei. In line with this supposition, a reasonably linear fit can be obtained between the squared isotropic displacements and the half-widths of the ortho protons (H_1) on the arylacetylide ligand in **1a**−**g**[PF_6] (Figure 8). For **1i**[PF_6] (X = OMe) and complexes with more electron-releasing substituents, the data start to deviate from this line

(40) Regarding the expression of δ_{pc} (eq 3), the following conditions are apparently verified: $\tau_r^{-1} < |g_{||} - g_{\perp}|\mu_B H\hbar^{-1}$ and $\tau_e \ll \tau_r$ (see later).[41]

(41) Jesson, J. P. *J. Chem. Phys.* **1967**, *47*, 579−581.

(42) Indeed, a clear deviation of the Curie law *is not observed* for all signals, as could be expected if temperature-independent and/or $1/T^n$-dependent ($n > 1$) terms were present in the expression of the paramagnetic shift due to GS degeneracy of closely lying excited states.[35a] Moreover, DFT computations on the various model complexes predict a nondegenerate ground state (GS) in which the gap between the singly occupied molecular orbital (SOMO) and the closest MO is larger than 2000 cm^{-1},[15] also in contradiction with low-lying excited states.[43]

(43) (a) Golding, R. M. *Pure Appl. Chem.* **1972**, *32*, 123−135. (b) Kurland, R. J.; McGarvey, B. R. *J. Magn. Reson.* **1970**, *2*, 286−301.

(44) (a) Köhler, F. H. *Z. Naturforsch.* **1974**, *29B*, 708−712. (b) Banci L. In *Biological Magnetic Resonance*; Berliner, L. J., Reuben, J., Eds.; Plenum Press: New York, 1993; Vol. 12, pp 79−111.

(45) In eq 7a, many symbols were already defined before:[34] r_M is the distance to the metal center in Å, ω_s is the spin angular frequency, $f_{dip}(\omega,\tau_c)$ and $f_{con}(\omega,\tau_e)$ represent the spectral density functions where τ_c and τ_e represent the various correlation times considered, while a_H is the hyperfine coupling constant with the proton under investigation (in J). Note also that Curie-type relaxation processes have been neglected in equation 7a, since they are often negligible for small complexes such as **1a**−**j**[PF_6]. Accordingly with this hypothesis, any line-broadening computed for a Curie-type dipolar relaxation process appears to be negligible when τ_r values are used as maximum estimates of τ_c.[17]

(46) The lack of clear (field)^2-dependence for all $\nu_{1/2}$ values excludes a dominant Curie-type dipolar relaxation as supposed while deriving equation 7a. Then, the nonconstant ratio between $\nu_{1/2}$ values for similar protons in two different complexes excludes a dominant dipolar relaxation process, while the lack of proportionality between the $\nu_{1/2}$ values and the corresponding squared contact shifts excludes a dominant contact mechanism.

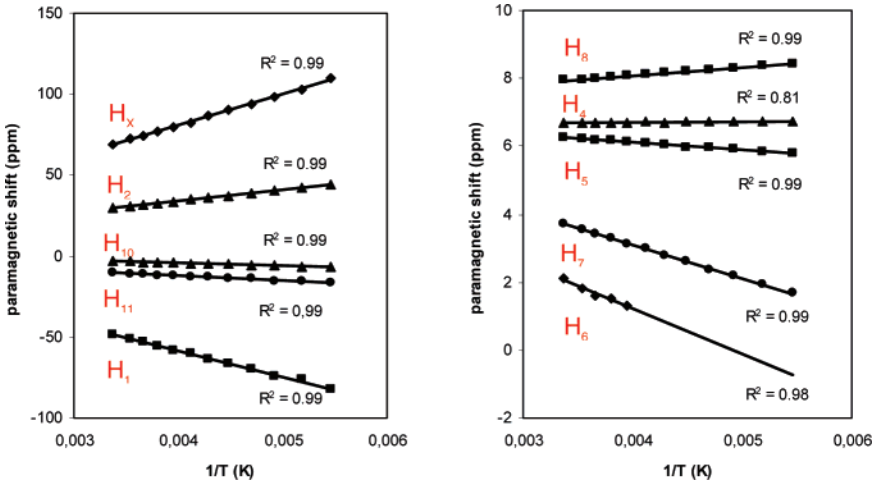

Figure 7. Temperature dependence of the ^{1}H NMR shifts of **1g**[PF_6] in CD_2Cl_2 with proposed assignment according to Chart 2.

Table 7. Comparison between the ^{1}H NMR Shifts (δ_{dia}) Recorded for 1a, 1g, and 2 at 20 °C and Those Extrapolated (δ_∞) from Shifts vs Temperature Plots Obtained with 1a[PF_6], 1g[PF_6], and 2[PF_6] in CD_2Cl_2

		C≡C−4-(C_6H_4)		dppe					C_5Me_5	X
compd		H_1	H_2	H_4	H_5	H_7	H_8	H_{10}	H_{11}	H_X
1a	δ_{dia}[a,b]	6.8	7.9	7.4	7.4	7.3	7.5	2.1	1.5	
1a[PF_6]	δ_∞[c]	−9.2	10.6	6.4	6.8	7.3	6.9	5.5	0.2	
	R^2[d]	0.99	0.99	0.97	0.99	0.99	0.99	0.99	0.99	
1g	δ_{dia}[a]	6.8	6.9	7.0−7.5	7.0−7.5	7.0−7.5	7.0−7.5	2.0	1.4	2.2
1g[PF_6]	δ_∞[c]	4.4	7.7	6.6	7.0	7.0	7.1	2.6	−1.0	4.7
	R^2[d]	0.99	0.99	0.81	0.99	0.99	0.99	0.99	0.99	0.99
2	δ_{dia}[a]			7.1−7.5	7.1−7.5	7.1−7.5	7.1−7.5	2.0	1.1	
2[PF_6]	δ_∞[c]			6.9	7.4	7.2	7.4	3.0	−8.5	
	R^2[d]			0.97	0.99	0.99	0.99	0.99	0.99	

[a] ^{1}H NMR shift at $T = 295$ K for the corresponding Fe(II) compound. [b] Complete attribution made by COSY and NOESY experiments on a 500 MHz spectrometer. [c] Extrapolated ^{1}H NMR shift at $T = \infty$. [d] Squared regression coefficients of the linear fits.

and are more accurately fitted by a logarithmic law, the compound **1g**[PF_6] (X = Me) constituting the limiting case for the linear dependence. This "logarithmic" dependence observed in Figure 8 most probably takes place because we neglected the dipolar contribution to the shift induced by local electron density in our treatment ($(\delta_{pc})^L$ in eq 2b). The latter becomes certainly quite important for the electron-releasing substituents, since quite sizable electronic densities are delocalized on the functional aryl ring (see DFT calculations section). As a consequence, the contact shift is derived in a more and more approximate way. Moreover, any local dipolar contribution to the line broadening was also neglected in eq 7a. These approximations certainly explain the nonlinear plot of Figure 8.

We next sought to obtain an estimate of the dipolar correlation time (τ_c) in eq 7a at ambient temperature with **1a**[PF_6], **1g**[PF_6], and **2**[PF_6]. An estimate of the rotational correlation time for **1a**−**j**[PF_6] and **2**[PF_6] can be readily obtained using the Stokes−Einstein formula (eq 8), where η is the viscosity of the medium ($0.423\ 10^{-3}$ kg m^{-1} s^{-1} at 298 K) and a is the mean radius of the molecule (8.46 and 10.36 Å, respectively). Values of $\tau_r = 4.8 \times 10^{-10}$ s and $\tau_r = 2.6 \times 10^{-10}$ s were respectively found for **1a**−**j**[PF_6] and **2**[PF_6].

$$\tau_r = 4\pi\eta a^3/3kT \qquad (8)$$

Then, still using these τ_r values as maximum estimates of τ_c along with r_M distances derived from X-ray structures, we have computed the theoretical line-broadening induced by dipolar relaxation for the two protons H_5 and H_8 of the dppe ligand in **1a**[PF_6], **1g**[PF_6], and **2**[PF_6]. The peaks of these protons present the smallest shifts and should therefore be only poorly broadened by contact relaxation. In line with a dominant dipolar relaxation mechanism, the half-widths of these ^{1}H NMR signals vary only slightly along the **1a**−**j**[PF_6] series. The computation of the dipolar line-broadening reveals that much larger half-widths should be experimentally observed, evidencing that the actual dipolar correlation times (τ_c) in **1a**[PF_6], **1g**[PF_6], and **2**[PF_6] must be lower than the rotational correlation times (τ_r) presently considered. In these compounds, τ_c appears therefore significantly influenced by τ_e (eq 7d). We found that dipolar correlation times around 7×10^{-11} s would produce the observed half-widths of H_5 and H_8 in **1a**[PF_6], **1g**[PF_6], and **2**[PF_6]. From these values, τ_e values slightly below 8.5×10^{-11} s can be inferred, but these are most probably high-lying estimates. Indeed, the half-widths computed using the τ_e values along with τ_r values previously determined (eq 8) are again larger than those experimentally observed for some other peaks, meaning that the correlation time (τ_c) of the dipolar relaxation process must be even shorter for these nuclei. The only way to reconcile this observation with experiment is that either (i) our supposition that the relaxation of H_5 and H_8 is mostly dipolar in origin was wrong or (ii) that a different "τ_e" operates for different protons. This can only be possible if the latter is in turn dependent on an "internal" correlation time (eq 9).[44b] Internal correlation times (τ_i), which can be as low as 10^{-12} s,[30,47] depend on intramolecular motions and can be different for various protons located on different fluxional groups. Whatever the exact reason, the τ_e values determined above constitute major values of τ_s in **1a**−**j**[PF_6] according to this reasoning. More sensible estimates can

(47) Jesson, J. P. *J. Chem. Phys.* **1967**, *47*, 582−591.

be obtained from the half-widths of H_1 (see Discussion section).

$$(\tau_e)^{-1} = (\tau_s)^{-1} + (\tau_i)^{-1} \quad (9)$$

Note that because of the much more important contribution of local dipolar effects on relaxation of other nuclei, similar information cannot be extracted so easily from the half-widths of the ^{13}C NMR and ^{19}F NMR signals. With these nuclei, much more complex expressions than eq 7a have to be considered in the general case.[38,48]

Self-Exchange Rates from Line-Broadening. As mentioned above, we were always under fast exchange conditions when making assignments from ^1H, ^{13}C, and ^{31}P NMR spectra from Fe(II)/Fe(III) mixtures. We therefore have sought to determine the self-exchange rates from line-broadening studies using Fe(II)/Fe(III) mixtures (Table 8). We used the classical formula given in eq 10a, which applies when $ck_e \gg (\Delta\delta)^2/ck_e \gg T_{2M}^{-1}$.[51] In this expression, c is the total concentration of reactants, $\Delta\delta$ is the difference in chemical shift between the two nonexchanging peaks expressed in Hz, and k_e is the self-exchange rate to be determined. To avoid any errors due to the temperature dependence of the Fe(III) proton shifts, $\Delta\delta$ values were estimated from spectra recorded at similar temperatures with pure samples of the Fe(II) and Fe(III) redox congeners. The self-exchange rates were determined from ca. $(3-4) \times 10^{-2}$ M solutions of the compounds in CD_2Cl_2, at several temperatures in the 300−190 K range.

$$W_{red,ox} = f_{red}f_{ox}4\pi(\Delta\delta)^2/ck_e \quad (10a)$$

$$f_{red} = (\delta_{ox} - \delta_{obs})/(\delta_{ox} - \delta_{red}) \text{ and } f_{ox} = 1 - f_{red} \quad (10b)$$

The rates were found to be in the range ca. 10.3×10^7 to 25.8×10^7 M^{-1} s^{-1} at ambient temperatures and are slightly substituent dependent, being apparently larger for electron-withdrawing substituents (Table 8). Notably, while eq 10a applies in principle only to noncoupled protons,[52] very similar results were presently found for most compounds either from the ^1H NMR peaks of the coupled H_1 and H_2 protons or from those of the C_5Me_5 peak. This is not surprising considering the rather large experimental uncertainty associated with these measurements due to inavoidable field inhomogeneities (±10%). We have also checked that these rates were independent of the counterion concentration.[52] Thus, similar rates were found for **2/2**[PF_6] mixtures when a fixed concentration (0.08 M) of [N^n-Bu_4][PF_6] was present in the reaction medium. The measurements were repeated at various temperatures, showing that the rates are slower at low temperatures. Activation energies around 11−12 kJ could be extracted from Eyring plots in each case (Table 8). Rates for **2**[PF_6] could not be determined below 230 K due to the excessive broadening of the C_5Me_5 signal, rendering the data extracted from Eyring plots less accurate for that particular compound.

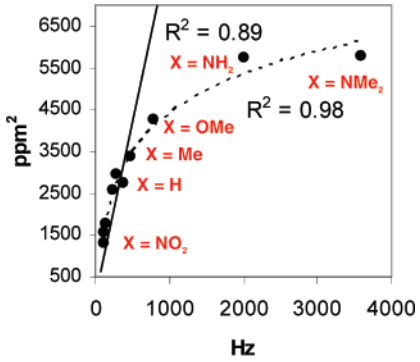

Figure 8. Correlation between $\nu_{1/2}$ (Hz) values and squared isotropic shifts (ppm²) for ^1H NMR signals of H_1 protons in **1a**−**j**[PF_6] complexes at 25 °C in CD_2Cl_2.

Table 8. Self-Exchange Rates (10^{-6} M^{-1} s^{-1}) as Determined from Line-Broadening Studies on the ^1H NMR Spectra for Selected Compounds among 1a−g[PF_6] and 2[PF_6] in CD_2Cl_2

	k_e (10^{-6} M^{-1} s^{-1})[a]			
compds	193 K	253 K	293 K	$\Delta H^{\ddagger}$ (kJ mol^{-1}/cm^{-1})
1a/1a[PF_6][b]	24	157	258	11.4/953
1b/1b[PF_6][c]	28	76	134	9.6/803
1c/1c[PF_6][c]	10	61	103	11.2/936
1g/1g[PF_6][b]	12	81	132	11.6/970
1h/1h[PF_6][c]	11	85	133	12.1/1011
2/2[PF_6][b]		23.9	41.8	8.6/718

[a] Values ± 15%. [b] Determined at 300 MHz. [c] Determined at 500 MHz.

Correlations of ^1H and ^{13}C NMR Shifts with Electronic Substituent Parameters (ESPs). During previous studies on **1a**−**j**[PF_6], we have shown that many characteristic properties of these compounds, such as ESR data,[15] can be linearly correlated using the σ^+ electronic substituent parameters (ESPs).[53,54] Again, if we except the data gathered for **1j**[PF_6], which most often is remote from the fit, rather similar linear dependences appear with isotropic (Figure 9a) or contact shifts. However, fits obtained here are overall poorer than those obtained with ESR data. This is not surprising considering the quite horizontal slopes of these linear correlations with respect to the experimental uncertainty on the shifts. In many cases, good correlations are also obtained using directly the uncorrected paramagnetic shifts measured against tetramethylsilane instead of the isotropic shift, as shown for the ^{13}C NMR shifts of the arylacetylide ligand in Figure 9b. As previously stated with ESR data, slightly poorer fits (not shown here) were obtained when the regular Hammett set was used instead of σ^+, suggesting the importance of mesomeric effects in these linear free-energy relationships (LFERs).

Theoretical (DFT) Spin Densities for Selected Fe(III) Model Complexes. Density functional theory (DFT) computations on Fe(III) were previously made on the model complexes **1a**-H^+ (X = NO_2), **1b**-H^+ (X = CN), **1d**-H^+ (X = Br), **1f**-H^+

(48) We have nevertheless checked that neither the dipolar nor the contact relaxation dominated the shifts of the ^{13}C NMR signals in **1a**−**j**[PF_6]. In the case of dominant metal-centered relaxation, we should have observed a constant linewidth for each signal of these carbon nuclei along the **1a**−**j**[PF_6] series, given the relative constancy of the geometric parameters. Alternatively, in the case of a dominant contact relaxation, a constant ratio depending on their respective contact shifts ($\nu_{1/2}(^{13}C_y)/\nu_{1/2}(^1H_x) \approx (\delta_C(^{13}C_y)/\delta_C(^1H_x))^2 \times (\gamma_C/\gamma_H)^2$) should be found for a given couple of peaks.[49] No such ratios were found when the ^{13}C NMR contact shifts were approximated by the corresponding isotropic shifts. Rather, the analysis of half-widths of the ^{13}C NMR signal of the arylacetylide ligand reveals the existence of rough correlations with the corresponding ^{13}C NMR isotropic shifts or with these quantities squared, in line with what is to be expected when the transverse relaxation rates are determined by either local dipolar effects or contact effects, or both.[50]

(49) Doddrell, D. M.; Gregson, A. K. *Chem. Phys. Lett.* **1974**, *29*, 512−515.

(50) (a) Doddrell, D. M.; Pegg, D. T.; Bendall, R.; Gottlieb, H. P. W. *Chem. Phys. Lett.* **1976**, *39*, 65−68. (b) Doddrell, D. M.; Healy, P. C.; Bendall, R. *J. Magn. Reson.* **1978**, *29*, 163−166.

(51) Simonneaux, G.; Bondon, A. *Chem. Rev.* **2005**, *105*, 2627−2646.

(52) Chan, M.-S.; Wahl, A. C. *J. Phys. Chem.* **1978**, *82*, 2542−2549.

(53) March, J. *Advanced Organic Chemistry. Reactions, Mechanisms and Structures*, 4th ed.; J. Wiley & Sons: New York, 1992.

(54) Hansch, C.; Leo, A.; Taft, R. W. *Chem. Rev.* **1991**, *91*, 165−195.

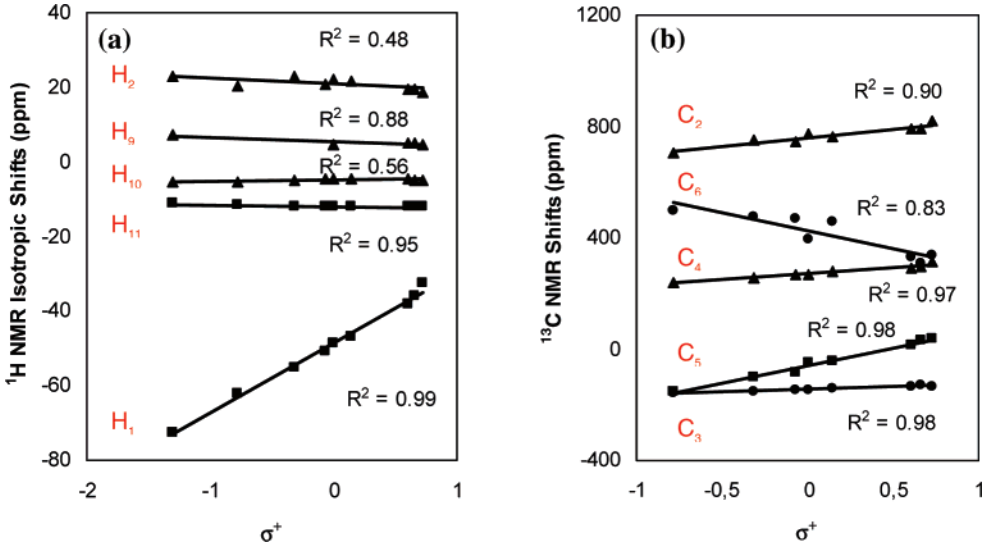

Figure 9. Plot of the ^{1}H NMR isotropic shifts (a) and the observed ^{13}C NMR shifts (b) of the arylacetylide nuclei in [(η^2-dppe)(η^5-C5Me5)Fe(C≡C)-4-(C_6H_4)X][PF_6] complexes (X = NO_2, CN, CF_3, F, Br, H, Me, OMe, NH_2) vs σ^+ ESPs.

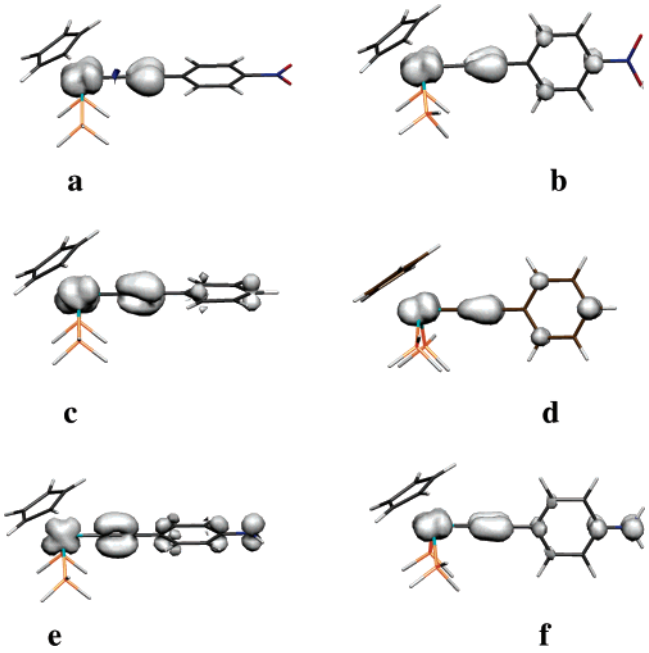

Figure 10. Plots of the total spin densities for $(H_3P)_2(\eta^5$-$C_5H_5)$-Fe(C≡C)-4-(C_6H_4)X complexes with parallel (left) and perpendicular (right) conformations of the arylalkynyl ligand. X = NO_2 (a,b); H (c,d); NH_2 (e,f). The contour values are 0.04 [e/bohr^3].

(X = H), **1h**-H$^+$ (X = OMe), and **1i**-H$^+$ (X = NH_2) in which the chelating dppe ligand had been replaced by two PH_3 ligands and the C_5Me_5 ligand by C_5H_5.[12,15] For these compounds the spin distribution had been computed in a conformation where the functional aryl group was roughly coplanar with the C_5H_5 ligand.[15]

We now have recalculated the spin densities for **1a**-H$^+$, **1f**-H$^+$, and **1i**-H$^+$ in a perpendicular conformation where the aryl group has been rotated 90°, and also in both conformations for the new model compound **1g**-H$^+$ where X = Me (Table 9). Importantly, for all Fe(III) model complexes investigated, the perpendicular conformation appears slightly more stable than the parallel one (Table 9). Notably, this trend is opposite the trend previously observed for selected Fe(II) parents.[12] For the purpose of comparison, spin densities were also derived for model complexes **1a**$^+$ and **1g**$^+$ featuring the complete coordination sphere.[55]

As shown in Table 10, the main difference with the computationally simpler model compounds **1a**-H$^+$ and **1g**-H$^+$ is that slightly more spin density is located on the metal center and on the surrounding atoms, in line with the improved electron-releasing nature of the coordination sphere of **1a**$^+$ and **1g**$^+$. Also, more spin density is delocalized in the acetylide spacer in comparison to the simpler model complexes **1a**-H$^+$ and **1g**-H$^+$, especially in the latter compound (Table 10). Notably, in spite of a more marked spin alternation in **1a**$^+$ and **1g**$^+$, the relative ratios between atomic densities on the functional aryl group are roughly the same as for **1a**-H$^+$ and **1g**-H$^+$ (Table 9), the discrepancies being slightly more pronounced between **1g**$^+$ and **1g**-H$^+$. In accordance with previous findings,[15] the largest positive spin density is always located on the metal center regardless of the conformation adopted, and then on the β-carbon atom (C_2) of the acetylide ligand.

As shown in Tables 9 and 10, the conformation of the arylalkynyl ligand has a sizable influence on the spin density residing on the metal center and on the arylacetylide ligand and has only a minor influence on the spin distribution in the phosphane and the cyclopentadienyl ligands. Notably, marked changes in the spin distribution within the aryl-alkynyl linker take place between the nitro compound conformers (**1a**-H$^+$ or **1a**$^+$), but this effect is apparently less pronounced for conformers of complexes possessing more electron-releasing substituents. This can be traced back to the different ordering of the frontier MOs possessing a strong metal character previously pointed out between compounds with strongly electron-withdrawing substituents, like **1a**-H$^+$ and compounds with more electron-releasing substituents.[15] As shown in Figure 11, the frontier spin orbitals with a strong d_{yz} character are slightly destabilized upon rotation of the aryl ring from the parallel to the perpendicular conformation. Conversely, frontier spin orbitals with a strong d_{xz} character are slightly stabilized. This leads to a crossing between the two metal-based frontier α spin orbitals, while the relative energy ordering of the β spin orbitals is not affected in **1a**-H$^+$. Thus, the electronic hole remains located in the π_y

(55) Given the much poorer match obtained with the amino complex **1i**-H$^+$ (see later), we did not compute the spin density for the model complex **1i**$^+$ presenting the exact coordination sphere.

Table 9. Calculated Spin Densities (e) on Selected Fragments or Atoms for $[(\eta^2\text{-dpe})(\eta^5\text{-}C_5H_5)FeCl]^+$ [27] (dpe = 1,2-diphosphinoethane) and $[(PH_3)_2(\eta^5\text{-}C_5H_5)Fe(C{\equiv}C{-}4{-}C_6H_4X)]^+$ Complexes (X = NO_2, H, NH_2) in Two Conformations (see Chart 4 for atom numbering)

					C≡C(C$_6$H$_4$)X							ΔE^a
R		Fe	C_5H_5	2 PH_3 (or dpe)	C_1	C_2	C_3	C_4	C_5	C_6	X	(kJ mol^{-1})
Cl		0.902	−0.023	−0.033[b]							0.154	
C≡C(C$_6$H$_4$)NO$_2$	∥[c]	0.799	−0.034	−0.026	−0.054	0.306	−0.027	0.013	0.000	0.000	0.010	14.0
	⊥[d]	0.640	−0.012	−0.027	−0.010	0.236	−0.033	0.085	−0.039	0.104	0.014	0
mean values		0.720	−0.023	−0.027	−0.032	0.271	−0.030	0.049	−0.020	0.052	0.012	
C≡C(C$_6$H$_5$)	∥[c]	0.637	−0.037	−0.034	0.042	0.241	0.001	0.056	−0.021	0.093	−0.007	*e*
	⊥[d]	0.578	−0.009	−0.014	0.030	0.222	−0.012	0.088	−0.039	0.137	−0.010	*e*
mean values		0.608	−0.023	−0.024	0.036	0.232	−0.006	0.072	−0.030	0.115	−0.009	
C≡C(C$_6$H$_4$)NH$_2$	∥[c]	0.400	−0.032	−0.038	0.145	0.125	0.073	0.040	0.026	0.088	0.127	17.4
	⊥[d]	0.436	−0.005	−0.023	0.089	0.148	0.050	0.045	0.018	0.084	0.106	0
mean values		0.418	−0.019	−0.031	0.117	0.137	0.062	0.043	0.022	0.086	0.117	

[a] Relative energy between the two conformations (kJ mol^{-1}). [b] Value for 1,2-diphosphinoethane (dpe). [c] Parallel conformation. [d] Perpendicular conformation. [e] For this compound, see Computational Details in the Experimental Section.

Table 10. Calculated Spin Densities (mean value in 10^3 e) for Selected Atoms in $[(\eta^5\text{-dppe})(\eta^5\text{-}C_5Me_5)Fe(C{\equiv}C{-}4{-}C_6H_4X)]^+$ and $[(PH_3)_2(\eta^5\text{-}C_5H_5)Fe(C{\equiv}C{-}4{-}C_6H_4X)]^+$ Complexes (X = NO_2: **1a$^+$, **1a**-H$^+$; Me: **1g**$^+$, **1g**-H$^+$) (see Chart 4 for atom numbering)**

compd		Fe	P	C_7(dppe)	C_{11}(dppe)	$C_{16}(C_5Me_5)$	X	ΔE^a
1a$^+$	∥[b]	926.8	−30.2	4.5	−0.1	−9.9	−0.2	6.8
	⊥[c]	851.8	−28.6	4.2	−0.1	−9.2	18.5	0
1a-H$^+$	∥[b]	799.5	−9.8			−8.0	10.1	14.0
	⊥[c]	639.8	−9.8			−3.0	18.7	0
1g$^+$	∥[b]	925.8	−30.6	4.8	0.1	−10.4	0.1	12.5
	⊥[c]	772.0	−26.8	38.5	−0.4	−8.3	4.0	0
1g-H$^+$	∥[b]	536.2	−21.2			−10.1	11.0	21.2
	⊥[c]	548.5	−9.5			−2.2	9.2	0

[a] Relative energy between the two conformations (kJ mol^{-1}). [b] Parallel conformation. [c] Perpendicular conformation.

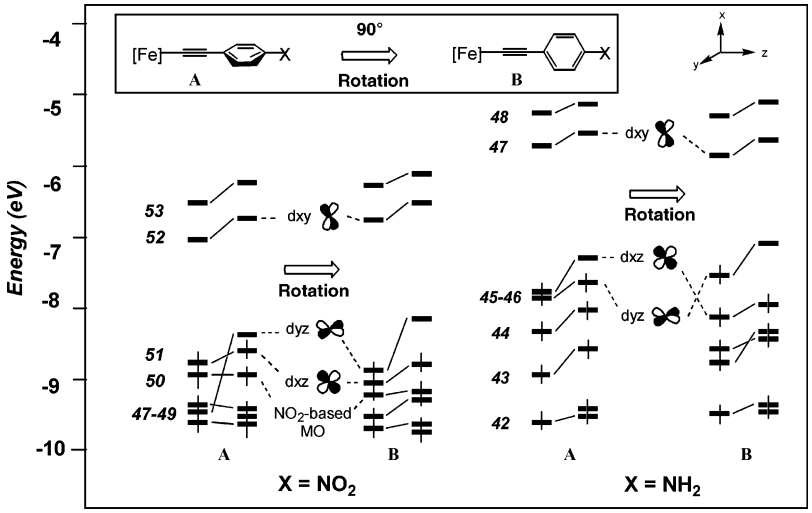

Figure 11. Evolution of the frontier spin-MOs of **1a**-H$^+$ (X = NO_2) and **1i**-H$^+$ (X = NH_2) after rotation of the functional aryl ring from parallel (∥) to perpendicular (⊥) conformation for $(H_3P)_2(\eta^5\text{-}C_5H_5)Fe(C{\equiv}C)$-4-$(C_6H_4)X$ complexes. The d-metal contribution is shown for the frontier spin orbitals with strong metal character.

manifold of the acetylide linker in both conformations. In addition, the lowest unoccupied β spin orbital becomes conjugated with the aryl ring in the perpendicular conformation and the unpaired electron is delocalized on the aryl ligand, while it was restricted to the acetylide spacer in the parallel conformation. For strongly electron-releasing substituents, a similar stabilization/destabilization of the frontier spin orbitals takes place upon rotation. This time, the crossing occurs for both the α and β manifolds (Figure 11). Consequently, the electronic hole "changes" MOs and a quite similar spin distribution results in both conformers. Finally, for compounds with moderately electron-releasing or -attracting substituents such as **1f**-H$^+$, the SOMO is a mixture of d_{yz} and d_{xz} AOs regardless of the conformation considered (Figure 10), and the rotation of the aryl ring does not markedly affect the spin delocalization.

Energy differences between 10 and 20 kJ mol^{-1} are computed between the two conformations for **1a**-H$^+$, **1f**-H$^+$, **1g**-H$^+$, and **1i**-H$^+$ (Table 9). Note that the steric interactions between neighboring ligands are not accounted for with such model compounds, presenting a simplified coordination sphere. Notably, significantly smaller energetic differences are found with the complexes **1a**$^+$ and **1g**$^+$, presenting the exact coordination sphere (Table 10). Whereas this might be due to a better evaluation of the steric interactions taking place between the

Table 11. Calculated Spin Densities ρ_C (10^3 e) for Selected Carbon Atoms in $[(PH_3)_2(\eta^5\text{-}C_5H_5)Fe(C{\equiv}C\text{-}4{-}C_6H_4X)]^+$ (X = NO_2, H, Me, NH_2) and in $[(\eta^5\text{-dppe})(\eta^5\text{-}C_5Me_5)Fe(C{\equiv}C{-}4{-}C_6H_4X)]^+$ Complexes (X = NO_2, Me) (when available, experimental spin densities are given for comparison)

	C≡C−4-(C_6H_4)−						X
	C_1[a]	C_2	C_3	C_4	C_5	C_6	C_X
			C≡C(C_6H_4)NO_2				
$(\rho_C)_{exp}$[b]				19	−9		
$(\rho_C)_{exp}$ ratios[c]				1.00	−0.47		
δ_C ratios[c,d]		3.81	−1.49	1.00	−0.46	1.07	
$(\rho_C)_{DFT}$ for **1a**-H^+[e]	−32	271	−30	49	−20	52	
$(\rho_C)_{DFT}$ ratios[c]	−0.65	5.53	−0.61	1.00	−0.41	1.06	
$(\rho_C)_{DFT}$ for **1a**$^+$[e]	−89	238	−34	38	−15	36	
$(\rho_C)_{DFT}$ ratios[c]	−2.31	6.21	−0.88	1.00	−0.40	0.94	
			C≡C(C_6H_5)				
$(\rho_C)_{exp}$[b]				28	−11	27[f]	
$(\rho_C)_{exp}$ ratios[c]				1.00	−0.39	0.96[f]	
δ_C ratios[c,d]		4.80	−1.98	1.00	−1.31	2.41	
$(\rho_C)_{DFT}$ for **1h**-H^+[e]	36	232	−6	72	−30	115	
$(\rho_C)_{DFT}$ ratios[c]	0.50	3.22	−0.08	1.00	−0.42	1.60	
			C≡C(C_6H_4)CH_3				
$(\rho_C)_{exp}$[b]				31	−12	31[g]	
$(\rho_C)_{exp}$ ratios[c]				1.00	−0.39	1.00[g]	
δ_C ratios[c,d]		4.98	−2.26	1.00	−1.83	2.72	−1.06
$(\rho_C)_{DFT}$ for **1g**-H^+[e]	77	189	13	80	−30	144	−10
$(\rho_C)_{DFT}$ ratios[c]	0.96	2.36	0.16	1.00	−0.38	1.80	−0.13
$(\rho_C)_{DFT}$ for **1g**$^+$[e]	−65	241	−26	38	−14	45	−3
$(\rho_C)_{DFT}$ ratios[c]	−1.69	6.31	−0.68	1.00	−0.37	1.17	−0.09
			C≡C(C_6H_4)NH_2				
$(\rho_C)_{exp}$[b]				40	−7		
$(\rho_C)_{exp}$ ratios[c]				1.00	−0.18		
δ_C ratios[c,d]				1.00			
$(\rho_C)_{DFT}$ for **1i**-H^+[e]	118	137	62	43	22	86	
$(\rho_C)_{DFT}$ ratios[c]	2.74	3.19	1.44	1.00	0.51	2.00	

[a] See Chart 4 for carbon atom numbering. [b] Determined from ^{1}H NMR contact shifts and McConnell equation (in 10^3 e). [c] Ratios relative to the C_4 carbon atom. [d] Ratios determined from the uncorrected isotropic ^{13}C NMR shifts. [e] Mean values between the parallel (∥) and perpendicular (⊥) conformations of the arylalkynyl ring (in 10^3 e). [f] Less precise value determined from "overlapping" para-H shift. [g] Less precise value determined from methyl shift and McConnell equation (see text).

Chart 5. Related Organic and Organometallic Radicals

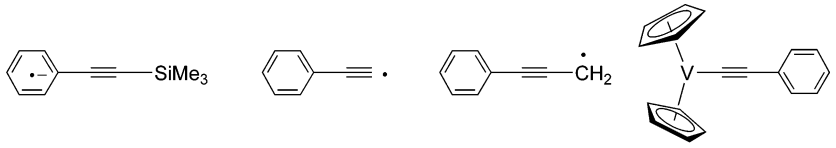

5$^-$ **6** **7** **8**

arylalkynyl hydrogen atoms and the cyclopentadienyl methyl groups in the latter set of compounds, the changes in electronic density on the metal center and within the acetylide linker in **1a**$^+$ and **1g**$^+$ certainly contribute as well to this decrease.

Discussion

Assignment of the Paramagnetic NMR Spectra. Most of the protons of **1a**−**k**[PF_6], **2**[PF_6], and **3a,b**[PF_6] (Chart 1) have been detected by NMR and were unambiguously assigned (Table 1). Notably, some previous assignments made for **2**[PF_6] and **1f**[PF_6] have been presently revised.[21,22] We have also shown here that protons H_3, H_4, H_5, and H_9 (Chart 2) exhibit slightly faster longitudinal (R_1) and transverse (R_2*) relaxation rates than H_6, H_7, H_8, and H_{10} (Supporting Information). These nuclei relax faster owing to large contributions of the dipolar mechanism to the relaxation process, due to their closer proximity to the metal center.

For the first time, these Fe(III) complexes were also studied by ^{13}C NMR. This is notable, given that studies on related organometallic complexes were rather scarce until now.[26,56] Again, most of the expected peaks for the various carbon nuclei for these compounds were detected, except for the nuclei lying closest to the metal atom such as the α-acetylide carbon (C_1) and the two ipso carbon atoms of the dppe ligand (C_7 and C_{11}). The failure to detect them most probably results from an excessive broadening induced by the proximity of the metal center. A similar statement was previously also made by Köhler et al. for paramagnetic V(III) arylacetylide complexes such as **8** (Chart 5).[26] In contrast, for compounds **1i**[PF_6] and **1j**[PF_6], bearing strongly electron-releasing substituents, many of the ^{13}C NMR signals pertaining to the aryl acetylide carbon atoms escaped detection (Table 2). This can be attributed to the larger spin densities delocalized on this ligand in these complexes, which in turn induces a faster relaxation of the ^{13}C nuclei by local dipolar effects. However, the β-acetylide carbon atoms (C_2), which present the largest spin densities of the compounds after the metal center (Tables 9 and 10), were always observed as very broad singlets in the 700−800 ppm range with **1a**−**h**[PF_6] (Table 2).

(56) Köhler, F. H. *J. Organomet. Chem.* **1974**, *64*, C27−C28.

Table 12. Calculated Spin Densities for H Atoms in $[(PH_3)_2(\eta^5\text{-}C_5H_5)Fe(C{\equiv}C{-}4{-}C_6H_4X)]^+$ (X = NO_2, H, Me, NH_2) and in $[(\eta^5\text{-dppe})(\eta^5\text{-}C_5Me_5)Fe(C{\equiv}C{-}4{-}C_6H_4X)]^+$ Complexes (X = NO_2, Me) (when available, experimental spin densities are given for comparison)

	C≡C−4−(C_6H_4)−		X
	H_1[a]	H_2	H_X
	C≡C(C_6H_4)NO_2		
$(\rho_H)_{exp}$[b]	−0.64	0.30	
$(\rho_H)_{exp}$ ratios[c]	1.00	−0.47	
δ_i ratios[c,d]	1.00	−0.57	
$(\rho_H)_{DFT}$ for **1a**-H^+ [e]	−3.7	1.8	
$(\rho_H)_{DFT}$ ratios[c]	1.00	−0.49	
$(\rho_H)_{DFT}$ for **1a**$^+$ [e]	−2.7	1.3	
$(\rho_H)_{DFT}$ ratios[c]	1.00	−0.46	
	C≡C(C_6H_5)		
$(10^3\ \rho_H)_{exp}$[b]	−0.93	0.36	−0.88
$(\rho_H)_{exp}$ ratios[c]	1.00	−0.39	0.95
δ_i ratios[c,d]	1.00	−0.45	1.00
$(\rho_H)_{DFT}$ for **1h**-H^+ [e]	−5.8	1.9	−8.5
$(\rho_H)_{DFT}$ ratios[c]	1.00	−0.33	1.46
	C≡C(C_6H_4)CH_3		
$(10^3\ \rho_H)_{exp}$[b]	−1.04	0.38	1.18
$(\rho_H)_{exp}$ ratios[c]	1.00	−0.37	−1.13
δ_i ratios[c,d]	1.00	−0.42	−1.22
$(\rho_H)_{DFT}$ for **1g**-H^+ [e]	−6.4	1.3	6.6
$(\rho_H)_{DFT}$ ratios[c]	1.00	−0.20	−1.03
$(\rho_H)_{DFT}$ for **1g**$^+$ [e]	−2.6	1.3	1.8
$(\rho_H)_{DFT}$ ratios[c]	1.00	−0.50	−0.69
	C≡C(C_6H_4)NH_2		
$(10^3\ \rho_H)_{exp}$[b]	−1.37	0. 25	−0.12
$(\rho_H)_{exp}$ ratios[c]	1.00	−0.18	0.09
δ_i ratios[c,d]	1.00	−0.20	0.08
$(\rho_H)_{DFT}$ for **1i**-H^+ [e]	−4.1	−2.1	−4.0
$(\rho_H)_{DFT}$ ratios[c]	1.00	−0.51	0.98

[a] See Chart 2 for proton numbering. [b] Determined from ^{1}H NMR contact shifts (in 10^3 e Å^{-3}). [c] Ratios relative to the value found for proton H_1. [d] Ratios determined from the uncorrected isotropic ^{1}H NMR shifts. [e] Mean values between the parallel (∥) and perpendicular (⊥) conformations of the arylalkynyl ring (in 10^3 e).

For related reasons, the detection of the ^{31}P signals of the dppe ligand for **1a**[PF_6] is quite remarkable as well. Indeed, only in rare instances were ^{31}P NMR peaks reported for paramagnetic complexes featuring a phosphane ligand directly coordinated to the metal center.[57] The large upfield shift observed for **1a**[PF_6] is sensible, since the isotropic hyperfine coupling constant ($|a_P|$) deduced from this isotropic shift (ca. 14 G) by neglecting the pseudocontact contribution is very similar to the mean diagonal value of the anisotropic hyperfine coupling tensor previously reported for [(η^2-dppm)(η^5-C_5Me_5)-FeC≡C−Ph][PF_6] ($|A_P|_{xx} \approx |A_P|_{yy} \approx |A_P|_{zz} \approx$ 14−15 G). Actually, this Fe(III) complex is the dppe analogue of **1f**[PF_6] and its $|A_P|$ values were measured by ESR.[58]

Spin Delocalization in Fe(III) Radicals. Regarding the spin distribution in these compounds, the ^{1}H NMR contact shifts in **1a**−**j**[PF_6] are clearly diagnostic of a sizable delocalization of the unpaired electron in a π MO of the arylacetylide ligand.[25,26] As expected from polarization effects operative in an alternant π manifold (Scheme 3), opposite shifts are observed for protons on adjacent carbon atoms. Also, ^{1}H NMR shifts in opposite directions are observed upon replacement of H_1 or H_2 by methyl groups (compare for instance the spectra of **1f**[PF_6] with those of **1g**[PF_6] or **3a,b**[PF_6]),[59] while substitution of the para (H_X) or meta (H_2) protons in **1f**[PF_6] for fluorine or trifluoromethyl substituents produces ^{19}F NMR shifts similar to those observed with fluorinated π-radicals.[40,60,61]

The $|a_H|$ values derived for the nuclei of the arylacetylide ligand (Table 4) are below those usually observed with purely organic aryl-centered radicals like the phenylalkynyl radical anion **5**$^-$ (Chart 5 and Table 13).[62] Also, the $|a_F|$ hyperfine constants derived for **1d**[PF_6] and ***m*-1d**[PF_6] (Table 3) are roughly one-third of those previously found for fluorinated phenoxy radicals.[63] Given that the unpaired electron density in **1a**−**j**[PF_6] is mostly localized on the metal center,[15] these Fe(III) complexes should preferably be compared with phenylalkynyl or γ-phenylpropargyl radicals like **6** and **7** (Chart 5), for which lower $|a_H|$ values were reported (Table 13).[64] Thus, the unpaired electron is approximately 4 time less delocalized on the aryl ring in **1a**−**j**[PF_6] than in **7**.

Also, in accordance with theoretical predictions, larger hyperfine constants are observed for the ortho (H_1) and para (H_X) protons than for meta (H_2) protons. This makes sense, since the carbon atoms C_4 and C_6 bearing these protons are conjugated with the metal center and consequently drain more spin density than do the meta carbon atoms (C_5) due to the occurrence of Fermi delocalization.[15] Along similar lines, the very slight difference in paramagnetic shift between the inequivalent H_1 or C_4 nuclei in ***m*-1d**[PF_6] can be understood considering that the fluorine substituent interacts in a π-fashion with an MO "orthogonal" to that containing the unpaired electron in this compound, thus inducing only a weak electronic perturbation on the shifts of these nuclei.

In comparison to the arylacetylide ligand, the spin delocalization in the η^5-C_5Me_5 and η^2-dppe ligands is lower. In **1a**−**j**[PF_6], the overall ^{1}H NMR shift to high field stated for the methyl groups reveals a large and negative spin density on the π manifold of the five-membered ring, in accord with DFT computations (Tables 9 and 10). In contrast, a positive spin density might be present within the σ-system of the C_5 ring according to the ^{13}C NMR shifts. The NMR data would therefore be in line with a σ-type spin delocalization mechanism.[65] Given the relative constancy of the geometric parameters, the pseudocontact contribution to the ^{1}H NMR shifts should not vary much between **1a**−**j**[PF_6] and **2**[PF_6]. Consequently, considering that the changes in the ^{1}H NMR and ^{13}C NMR shifts of the η^5-C_5Me_5 ligand mostly originate from changes in the contact contribution, the isotropic NMR shifts tend to indicate that the spin density on the cyclopentadienyl ligand has slightly increased upon proceeding from **1a**−**j**[PF_6] to **2**[PF_6]. In line with such a hypothesis, the half-widths of the peak of the methyl group from the cyclopentadienyl ligand observed for **2**[PF_6] are significantly broader (ca. 2115 Hz) in comparison to the corresponding ^{1}H NMR signals for **1a**−**j**[PF_6] or **4**[PF_6] (≤775 Hz). This also suggests that the arylacetylide ligand competes more efficiently

(57) Mink, L. M.; Polam, J. R.; Christiensen, K. A.; Bruck, M. A.; Walker, F. A. *J. Am. Chem. Soc.* **1995**, *117*, 9329−9339.
(58) Connelly, N. G.; Gamasa, M. P.; Gimeno, J.; Lapinte, C.; Lastra, E.; Maher, J. P.; Le Narvor, N.; Rieger, A. L.; Rieger, P. H. *J. Chem. Soc., Dalton Trans.* **1993**, 2575−2578.
(59) (a) Lazdins, D.; Karplus, M. *J. Am. Chem. Soc.* **1965**, *24*, 920−921. (b) Forman, A.; Murrell, J. N.; Orgel, L. E. *J. Chem. Phys.* **1959**, *31*, 1129, and references therein.
(60) Eaton, D. R.; Josey, A. D.; Benson, R. E.; Phillips, W. D.; Cairns, T. L. *J. Am. Chem. Soc.* **1962**, *84*, 4100−4106.
(61) Icli, S.; Kreilick, R. W. *J. Phys. Chem.* **1971**, *75*, 3462−3465.
(62) (a) Evans, A. G.; Evans, J. C.; Phelan, T. J. *J. Chem. Soc., Perkin Trans. 2* **1974**, 1216−1219. (b) Evans, A. G.; Evans, J. C.; Emes, P. J.; Phelan, T. J. *J. Chem. Soc. B* **1971**, 315−318.
(63) Espersen, W. G.; Kreilick, R. W. *Mol. Phys.* **1969**, *6*, 407−416.
(64) (a) Coleman, J. S.; Hudson, A.; Root, K. D. J.; Walton, D. R. M. *Chem. Phys. Lett.* **1971**, *11*, 300−301. (b) Kochi, J. K.; Krusic, P. J. *J. Am. Chem. Soc.* **1970**, *92*, 4110−4114.
(65) Rettig, M. F. In *NMR of Paramagnetic Molecules*; La Mar, G. N., Horrocks, D., Holm, R., Eds.; Academic Press: New York, 1973; pp 217−242.

with the η^5-C_5Me_5 ligand in **1a**−**j**[PF_6] than does the chloride ligand in **2**[PF_6] for delocalizing the unpaired electron. Thus, it is the arylacetylide linker and not the C_5Me_5 ligand that most strongly contributes to the delocalization of the unpaired electron in **1a**−**j**[PF_6].[22] Other experimental facts in agreement with this proposal are the much larger shifts observed for the protons of the para-phenyl substituent shifts in **4**[PF_6] in comparison to those of the aromatic dppe signals.

Regarding the diphosphine ligand, the ^{31}P NMR shift to high field observed for **1a**[PF_6] clearly reveals the presence of a negative spin density on the phosphorus nuclei, which most likely results from polarization effects, according to the DFT calculations (Tables 9 and 10). Due to their low magnitude, the ^{1}H NMR contact shifts for protons of the dppe ligand should be interpreted more cautiously, especially without any accurate determination of the pseudocontact shifts.[66] The DFT calculations indicate that only a slight amount of negative spin density is directly delocalized from the phosphorus atoms to the phenyl rings by Fermi contact. Although the π manifold certainly contributes to this process, part of the contact shift also originate from unpaired spin density in the σ manifold, since the typical alternation between the ^{1}H NMR shifts of vicinal protons is not observed for the aromatic protons H_3−H_5 and H_6−H_8 (Table 1).[68] Such behavior is apparently common for arylphosphine ligands bound to paramagnetic metal centers.[69]

Similar to eq 5, an equation can be written for the fluorine ^{19}F isotropic constants (eq 11). In that case, due to the presence of a p-type AO on the fluorine, polarization effects must be accounted for (eq 11).[17] Using eq 11 in combination with eq 4 and the carbon spin densities of **1f**[PF_6],[70] along with the $(Q_{app})^F$ values previously proposed by Eaton and co-workers ($(Q_{app})^F$ = 73.8 G/*m*-F, 52.6 G/*p*-F, 38.4 G/*p*-CF_3),[60,71] the ^{19}F NMR contact shifts were computed for **1c**[PF_6], **1d**[PF_6], and ***m*-1d**[PF_6] and amount to 94.7, 128.0, and −75.5 ppm, respectively. These shifts are clearly different from the shifts found when the isotropic shift is simply corrected for the metal-centered pseudocontact contribution (45.5, 132.5, and −21.8 ppm), but have the correct sign. Thus, if the constants used in eq 11 are indeed appropriate for these compounds,[63] this constitutes another indication of the existence of additional non-negligible ligand-centered pseudocontact contributions $(\delta_{pc})^L$ to the ^{19}F NMR isotropic shifts. Such effects were previously neglected by Eaton and co-workers.

$$a_F = (Q_{CF})^C(\rho_C)^\pi + [(S_F)^F + (Q_{FC})^F](\rho_F)^\pi = \{(Q_{CF})^F + Ap_{CF}[(S_F)^F + (Q_{FC})^F]\}(\rho_C)^\pi = (Q_{app})^F(\rho_C)^\pi \quad (11)$$

Comparison between Spin Densities Derived from the Experiment (NMR) and Theory (DFT). Spin densities for carbon nuclei were derived from ^{1}H NMR contact shifts using the McConnell equation (eq 5) and for protons using eq 12 in combination with eq 4.[17,72] As shown in Table 11, the spin densities determined experimentally using McConnell's expression were in general smaller than those computed by DFT. This is not surprising considering that DFT has a tendency to overestimate spin delocalization.[73] For comparison purposes, their relative ratios were therefore also given in Tables 11 and 12.

$$a_H = (2\mu_0/3)(\hbar\gamma_H g_e \mu_B)\rho_H \quad (12)$$

In line with the weak energetic differences (below 22 kJ mol^{-1}) computed between the parallel and perpendicular conformations for **1a**-H^+, **1f**-H^+, **1g**-H^+, and **1j**-H^+ (Tables 9 and 10), facile rotation of the aryl ring can be anticipated at ambient temperature. Accordingly, variable-temperature NMR experiments performed on selected Fe(II) samples suggest that the arylalkynyl ligand is rotating freely in solution down to 200 K.[30] In order to compare computed spin densities with spin densities deduced from NMR measurements in solution, the average between the theoretical spin densities calculated for the two conformers was taken into consideration (Tables 11 and 12).

Regarding spin densities on the protons of the arylacetylide ligand, it can be stated that ratios between empiric values obtained for the spin densities compare remarkably well with theoretical (DFT) values computed in the case of complexes bearing an electron-withdrawing substituent like **1a**[PF_6], and this is regardless of the accuracy of the model compound used in the calculations (**1a**-H^+ or **1a**$^+$). The match is excellent, especially when considering the approximations made during their experimental determination along with the inherent precision of DFT computations where no solvent nor counterion was considered (Tables 11 and 12).[74] In contrast, for the compound **1j**-H^+ with a strongly electron-releasing substituent, the match is much poorer. Several explanations can be put forward to rationalize this discrepancy. First, it was noticed earlier that when the substituent becomes more electron-releasing, larger differences between computed spin distributions are found for the arylacetylide ligand between model complexes featuring the exact coordination sphere and simpler model complexes. Thus, **1j**-H^+ might be less adapted than a more accurate model compound like **1j**$^+$ for computing the spin densities in these cases. Then, for complexes bearing electron-releasing substituents, the non-negligible influence of local dipolar effects on the isotropic shifts has also been previously put forward (Figure 8). The importance of such effects on relaxation rates has been discussed by Doddrell and co-workers.[49,50] However, estimation of their influence on the isotropic shifts is outside the scope of this work, since it is far from being trivial.[75] Thus, given that these effects are not accounted for in the classical treatment used here, an increasingly wrong contact shift is possibly determined from experiment by our approach (eq 3) for compounds with strongly electron-withdrawing substituents.

(66) As pointed out by one referee, for compounds exhibiting a slight rhombic distortion of the *g* tensor, equations making use of the susceptibility anisotropy values should have been used instead of eq 3.[17] However, in order to obtain very accurate values of the metal-centered pseudocontact shifts, a weighted average of all different conformations of the compounds should also have been considered.[67] This proved clearly unfeasible with such labile compounds, especially considering the large number of degrees of freedom of the dppe ligand in these complexes (see for instance Scheme 2).

(67) Horrocks, W. D., Jr.; Greenberg, E. *Inorg. Chem.* **1971**, *10*, 2190−2194.

(68) Horrocks, W. D., Jr.; Taylor, R. C.; La, Mar, G. N. *J. Phys. Chem.* **1964**, *86*, 3031−3038.

(69) (a) Doddrell, D. M.; Roberts, J. D. *J. Am. Chem. Soc.* **1970**, *92*, 6839−6844. (b) Moroshima, I.; Yonezawa, T.; Goto, K. *J. Am. Chem. Soc.* **1970**, *92*, 6651−6653.

(70) It was often proposed that hydrogen for fluorine substitution does not affect the π-spin density on the adjacent carbon atom.[39,71]

(71) Eaton, D. R.; Josey, A. D.; Phillips, W. D.; Benson, R. E. *Mol. Phys.* **1962**, *5*, 407−416.

(72) In this expression, ρ_H is the spin density residing in the s orbital of the observed H nucleus. Other symbols have their usual meaning, which was defined previously.[34]

(73) Ciofini, I.; Illas, F.; Adamo, C. *J. Chem. Phys.* **2004**, *120*, 3811−3816, and references therein.

(74) Adamo, C; Subra, R.; Di Matteo, A.; Barone, V. *J. Chem. Phys.* **1998**, *109*, 10244−10254.

(75) Gottlieb, H. P. W.; Barfield, M.; Doddrell, D. M. *J. Chem. Phys.* **1977**, *67*, 3785−3794.

Scheme 3. Qualitative Spin Distribution on the Arylacetylide Ligands Deduced from the ^{1}H NMR Contact Shifts

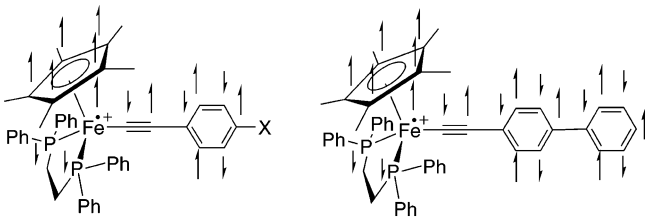

1a-k$^+$ **4$^+$**

Table 13. Hydrogen Hyperfine Coupling Constants (G) with Aryl Protons Determined for Various Organic Aryl-Based Radicals at Different Temperatures

compd	T (K)	$\lvert a_H\rvert_{ortho}$	$\lvert a_H\rvert_{meta}$	$\lvert a_H\rvert_{para}$
5[K]	193	0.16	3.16	7.49
6	273−263	2.22	0.81	2.16
7	<273	2.55	0.82	2.55

This, in turn also certainly contributes to overestimating the real spin density on carbon nuclei such as C_4.

The good agreement observed between computed DFT values and carbon spin densities ratios deduced using the McConnell equation in most compounds among **1a**−**j**[PF_6] (Table 11) is also worth mentioning.[74] This indicates that a $\pi-\sigma$ polarization mechanism dominates the NMR contact shifts of the arylacetylide protons and, in accordance with calculations, confirms that the unpaired electron is mostly delocalized on the π manifold of the arylacetylide ligand. Indeed, such a good correspondence should not be obtained if a sizable direct spin delocalization had taken place via the σ manifold. Regarding the arylacetylide nuclei, we also show (Table 12) that fair relative estimates of the atomic spin densities can already be obtained from ratios between uncorrected isotropic ^{1}H NMR shifts. This is however clearly not the case for the corresponding ^{13}C NMR isotropic shifts (Table 11). Due to the existence of p-type AOs on carbon nuclei, these shifts constitute far less reliable indicators of atomic spin densities due to the contribution of polarization effects along with non-negligible local dipolar effects.

Köhler and co-workers have previously shown that the conformation adopted by the aryl ring in the arylacetylide ligand can have a strong influence on the spin delocalization within this ligand (Figure 10).[56] Likewise with **1a**−**i**$^+$ complexes, DFT calculations suggest that the changes in spin distribution between the two conformations will be especially marked for compounds bearing strongly electron-withdrawing substituents such as **1a**$^+$ (Scheme 4). In other cases, the electronic relaxation after rotation results in a quite analogous spin distribution in parallel and perpendicular conformations. Thus, at least in compounds with electron-withdrawing substituents like **1a**[PF_6], the rotation of the phenyl ring does slightly modulate the spin density on the metal center and on the C_5Me_5 ring. For these compounds, the internal correlation time (τ_i) associated with this motion might therefore influence the correlation time (τ_c) corresponding to the dipolar relaxation of nuclei on other ligands (eq 9).

Substituent Influence on Spin Delocalization. To our knowledge, while substituent effects on the NMR shifts have previously been investigated for diamagnetic organic alkynes,[76] no such investigations have been conducted for paramagnetic alkynyl complexes. For **1a**−**h**[PF_6], both DFT calculations on model compounds and ^{1}H NMR shifts clearly confirm that the unpaired spin density will spread more and more on the arylalkynyl ligand in proportion to the electron-releasing capability of the para substituent. Further, the observed linear correlations with σ^+ ESPs (Figure 9) suggest that it results from a purely electronic substituent effect, depending largely on the π-interaction of the X substituent with the aryl ring. On the basis of these correlations, it seems clear that NMR provides a simple way to check the nature of an unknown para substituent in similar compounds. However, this linear dependence apparently breaks down for complexes bearing very electron-releasing substituents such as **1j**[PF_6], an observation that might again be related to the existence of strong local dipolar effects.

Note that usual ESP sets are traditionally considered as reflecting substituent-induced changes in charge distribution within the functional aryl group, *not changes in spin distribution*.[54,77] Although we could not find any proportionality between the computed Hirschfeld charges and spin densities for any Fe(III) model complex presently investigated, a rough correspondence between the substituent-induced changes for these two data sets along the **1a**-H$^+$/**1j**-H$^+$ series was apparent for C_1, C_2, and C_3 (Supporting Information).[12] In line with this observation, approximate linear correlations between the computed spin densities and the σ^+ ESPs were also found (Figure 12) for these nuclei. This can presently explain the linear free energy relationships (LFER) observed with the ^{1}H NMR isotropic shifts. However, the spin and charge variations induced by the substituents on C_4−C_6 are much smaller. In regard to the accuracy of the DFT method, further rationalization of the observed LFERs on the basis of the present calculations is therefore quite tentative (Figure 9a).

Linewidth Data and Self-Exchange Rates. A maximum value of the electronic correlation time ($\tau_e < 8.5 \times 10^{-11}$ s) was derived above from the linewidths of the ^{1}H NMR peaks of **1a**[PF_6] and **1g**[PF_6] according to Bloembergen−Solomon-like expressions (eqs 7a−d).[78] Now, considering that the half-widths of the ortho-acetylide protons (H_1) are solely determined by the contact relaxation (see above), these values in **1a**[PF_6] and **1g**[PF_6] can be further precised, although the latter complex constitutes obviously a limiting case for such an approach, due to the neglect of any local dipolar effect on the proton spin relaxation (Figure 8). Values around 2.2×10^{-11} and 3.5×10^{-11} s can thus be derived for τ_e, respectively. Considering the non-negligible energy differences found by DFT between the two extreme conformations of the aryl ring (Table 10), we can suppose that for H_1 and H_2 the rotation rate of the aryl ring around the acetylide axis is much slower than the electron spin relaxation ($\tau_i \gg \tau_s$). In the absence of other internal motion (see eq 9), the electronic correlation time presently determined therefore roughly corresponds to the spin correlation time (τ_s) under the assumption of equal longitudinal and transverse relaxation times ($\tau_s \approx \tau_{1s} \approx \tau_{2s}$).[17] Thus τ_e would roughly correspond to the relaxation time of the unpaired electron (τ_s), for which values around $(2-4) \times 10^{-11}$ s can be proposed. Actually, these estimates are somewhat higher than most τ_s values that were previously reported for low-spin Fe(III) complexes (closer to 10^{-12} s).[17] However, to our knowledge, essentially purely inorganic Fe(III) complexes were investigated in terms of τ_s until now, not organometallic ones such as **1a**−**j**[PF_6]. Moreover, the data tend to indicate that τ_s values slightly

(76) Rubin, M.; Trofimov, A.; Gevorgyan, V. *J. Am. Chem. Soc.* **2005**, *127*, 10243−10249, and references therein.

(77) (a) Jiang, X.-K. *Acc. Chem. Res.* **1997**, *30*, 283−289. (b) Shorter, J. *Chem. Z.* **1985**, *19*, 197−208. (c) Jaffé, H. H. *Chem. Rev.* **1953**, *53*, 191−261.

(78) (a) Solomon, I. *Phys. Rev.* **1955**, *99*, 559−566. (b) Bloembergen, N. *J. Chem. Phys.* **1957**, *27*, 572−573. (c) Bloembergen, N.; Purcell, E. M.; Pound, R. V. *Phys. Rev.* **1948**, *73*, 679−715.

Scheme 4. Changes in SOMO in the Two Conformations Resulting from a 90° Rotation of the Aryl Ring in 1a−j[PF$_6$] for Strongly Electron-Withdrawing Substituents (A) and in Other Cases (B)

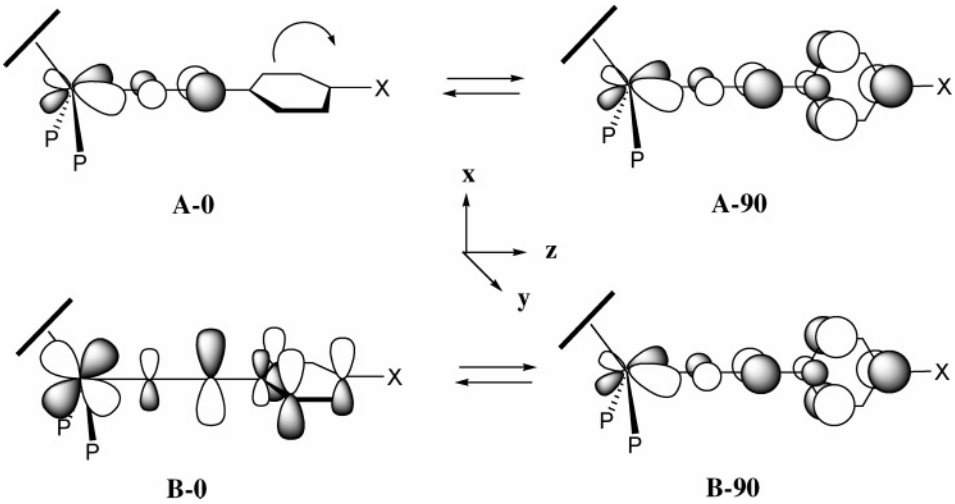

increase when the substituent becomes more electron-releasing, in accordance with ESR measurements.[15]

Self-exchange rates for several redox couples were also derived from half-widths of Fe(II)/Fe(III) mixtures at various temperatures. The rates found range from ca. 10×10^7 to 25.8×10^7 M^{-1} s^{-1} at 25 °C. These rates are faster for **1a**−**j**[PF$_6$] than for **2**[PF$_6$], and among **1a**−**j**[PF$_6$] appear faster for complexes with electron-withdrawing substituents. Activation energies around 9−12 kJ mol^{-1} were derived for these processes (Table 8). The close similarity between these values suggests that the changes in self-exchange rates among **1a**−**j**[PF$_6$] are not solely determined by changes in the corresponding activation energies, but that they will also strongly depend on differences in the Arrhenius prefactors. Unfortunately, given that Arrhenius prefactors are obtained from Eyring plots with very large uncertainties, no further rationalization of the substituent influence on the self-exchange rates was attempted. In comparison to other families of redox couples, the self-exchange rates found for **1a**−**j**[PF$_6$] or **2**[PF$_6$] are slightly faster than these previously determined for tris-diimine cationic iron complexes such as [Fe(bipy)$_3$]$^{3+}$/[Fe(bipy)$_3$]$^{2+}$,[52] but much faster than self-exchange rates reported for anionic hexacyano complexes such as [Fe(CN)$_6$]$^{3-}$/[Fe(CN)$_6$]$^{4-}$.[79] Considering an outer-sphere process with negligible electronic coupling, reorganization energies around 4000 cm^{-1} can be deduced from the activation energies of these electron-transfer reactions.[51,80] Such low reorganization energies were expected from previous investigations on **1a**-**j**[PF$_6$].[12,14] Actually, these values compare quite well with values around 4000−5000 cm^{-1} derived for related dinuclear complexes in the mixed-valent Fe(II)/Fe(III) state from the intervalence charge-transfer (IVCT) bands.[10a] This suggests that the electronic reorganization taking place during the electron-transfer event involves primarily the "(η^2-dppe)(η^5-C$_5$Me$_5$)FeC≡C−" fragment.

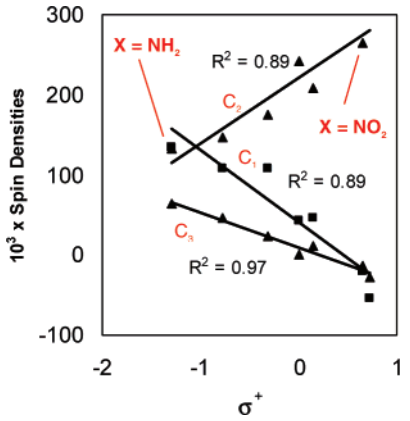

Figure 12. Plot of the computed spin density for selected carbon atoms of the arylacetylide nuclei in [(PH$_3$)$_2$(η^5-C$_5$H$_5$)Fe(C≡C)-4-(C$_6$H$_4$)X]$^+$ complexes (X = NO$_2$, CN, Br, H, Me, OMe, NH$_2$) vs σ^+ ESPs.

Conclusions

Several paramagnetic Fe(III) mononuclear arylacetylide complexes of formula (η^2-dppe)(η^5-C$_5$Me$_5$)Fe−C≡C−Ar (Ar = functional aryl group) were studied by multinuclear NMR. The signals of most of the nuclei could be detected, and a complete assignment of the various ^{1}H, ^{13}C, and in some cases ^{19}F signals was proposed for the corresponding NMR spectra. It clearly appears from this work that the arylacetylide linker and not the permethylated cyclopentadienyl ligand quite strongly contributes to the delocalization of the unpaired electron in **1a**−**j**[PF$_6$], in contrast to what was previously found for **2**[PF$_6$]. In connection with this observation, we show here that the ^{1}H NMR shifts of the ortho (H_1) and meta (H_2) arylacetylide protons can be interpreted in terms of dominant contact contribution and bring decisive information on the spin distribution within the aryl ring for most compounds investigated using fairly simple treatments. Estimates of the proton (a_H) and fluorine (a_F) hyperfine coupling constants were therefore derived for nuclei of the arylacetylide linker. These data are diagnostic of an unpaired electron dominantly centered on the metal center and partly residing in a π MO on the arylacetylide ligand. All these statements are also well substantiated by DFT calculations on computationally simpler model compounds. Sensible estimates of the electronic relaxation times around 2×10^{-11} s could be derived from the half-widths of the various ^{1}H NMR peaks of **1a**−**j**[PF$_6$] at ambient temperatures. An important finding of this work is also that quite sizable contributions to the ^{1}H NMR isotropic shifts might come from local dipolar effects due to the relatively large

(79) Shporer, M.; Ron, G.; Loewenstein, A.; Navon, G. *Inorg. Chem.* **1965**, *4*, 361−364.

(80) (a) Brunschwig, B. S.; Creutz, C.; Sutin, N. *Chem. Soc. Rev.* **2002**, *31*, 168−184. (b) Nelsen, S. F.; Blackstock, S. C.; Kim, Y. *J. Am. Chem. Soc.* **1987**, *109*, 677−682. (c) Creutz, C.; Newton, M. D.; Sutin, N. *J. Photochem. Photobiol. A* **1994**, *82*, 47−59.

spin density present on the arylacetylide ligand in compounds bearing electron-releasing substituents. Finally, estimates of the self-exchange rates in the $(10-26) \times 10^7$ M^{-1} s^{-1} range were derived for these complexes from line-broadening studies of Fe(II)/Fe(III) mixtures. These self-exchange rates are slightly substituent dependent and are apparently faster for the compounds with electron-withdrawing groups. Reorganization energies around 4000 cm^{-1} could be obtained for the associated electron-transfer process, which compare quite well with previous estimates of similar quantities in related dinuclear mixed-valent complexes. In conclusion, the present contribution clearly shows that multinuclear NMR constitutes a very powerful tool to study paramagnetic electron-rich Fe(III) acetylide complexes with $S = 1/2$ such as **1a**−**g**[PF_6] in solution. Provided the appended substituent is not too strongly electron-releasing, this technique allows mapping the spin distribution in such compounds in a quite straightforward way.

Experimental Section

General Data. All manipulations were carried out under inert atmospheres. Solvents or reagents were used as follows: Et_2O and *n*-pentane, distilled from Na/benzophenone; CH_2Cl_2, distilled from CaH_2 and purged with argon; $HN(^iPr)_2$, distilled from KOH and purged with argon; aryl bromides (Acros, >99%), opened/stored under Ar. The [(η^5-C_5H_5)$_2$Fe][PF_6] ferricinium salt was prepared by previously published procedures.[81] Transmittance-FTIR spectra were recorded using a Bruker IFS28 spectrometer (400−4000 cm^{-1}). Raman spectra of the solid samples were obtained by diffuse scattering on the same apparatus and recorded in the 100−3300 cm^{-1} range (Stokes emission) with a laser excitation source at 1064 nm (25 mW) and a quartz separator with a FRA 106 detector. Near-infrared (NIR) spectra were recorded using a Bruker IFS28 spectrometer, using a Nernst Globar source and a KBr separator with a DTGS detector (400−7500 cm^{-1}), a tungsten source and a quartz separator with a Peltier-effect detector (5200−12500 cm^{-1}), or on a Cary 5 spectrometer (4000−12500 cm^{-1}). UV−visible spectra were recorded on an Uvikon XL spectrometer (250−12500 cm^{-1}). All NMR experiments were made on a Bruker Avance 500 operating at 500.15 MHz for ^{1}H, 125.769 MHz for ^{13}C, and 201.877 MHz for ^{31}P, with a 5 mm broadband probe equipped with a z-gradient coil. More details about the NMR experiments are provided as Supporting Information. ESR spectra were recorded on a Bruker EMX-8/2.7 (X-band) spectrometer. Cyclic voltammograms were recorded using a EG&G potentiostat (M.263) on platinum electrodes referenced to an SCE electrode and were calibrated with the Fc/Fc^+ couple taken at 0.46 V in CH_2Cl_2.[81] MS analyses were performed at the "Centre Régional de Mesures Physiques de l'Ouest" (CRMPO, University of Rennes) on a high-resolution MS/MS ZABSpec TOF micromass spectrometer. Elemental analyses were performed at the CRMPO or at the Centre for Microanalyses of the CNRS at Lyon-Solaise, France.

Complexes **1a**−**j**[PF_6][15] and **4**[PF_6][10a] were obtained as previously reported, and the new complex ***m*-1d**[PF_6] was obtained following a similar route from the known ***m*-1d** Fe(II) precursor.[28] The organic arylacetylides **5a**,**b** were synthesized following classical routes either from trimethylsilyl acetylene and meta-xylyl bromide via a Sonogashira coupling protocol for **5a**[82] or via a Wittig procedure from mesityl aldehyde and the corresponding dibromocarbene phosphonium salt followed by in situ dehydrohalogenation for **5b**.[83]

Synthesis of the Mononuclear Fe(II) Alkynyl Complex (η^2-dppe)(η^5-C_5Me_5)Fe−C≡C-3,5-(C_6H_3(CH_3)$_2$) (3a). (η^2-dppe)(η^5-C_5Me_5)Fe(Cl) (**2**, 1.000 g, 1.60 mmol), NH_4PF_6 (0.315 g, 1.93 mmol), and (3,5-dimethylphenyl)acetylene (0.360 g, 2.77 mmol) were suspended in 50 mL of methanol, and the mixture was stirred 12 h at 25 °C. After concentration to 10 mL and decantation, the orange solid was filtrated, washed with methanol (5 mL), and extracted with 50 mL of dichloromethane. Concentration of the extract (2 mL) and precipitation by excess diethyl ether (20 mL) allowed the isolation of [(η^2-dppe)(η^5-C_5Me_5)Fe=C=CH{3,5-(C_6H_3)(CH_3)$_2$}][PF_6] (**7a**[PF_6]) as an air-sensitive orange solid (1.020 g, 1.182 mmol, 74%). This vinylidene complex (0.800 g, 0.927 mmol) was then stirred for 3 h in THF in the presence of excess potassium *tert*-butoxide (0.157 g, 1.391 mmol). After removal of the solvent and extraction with toluene, concentration of the extract to dryness, and subsequent washings with *n*-pentane, the desired orange (η^2-dppe)(η^5-C_5Me_5)Fe[C≡C-3,5-(C_6H_3)(CH_3)$_2$] complex **3a** was obtained (0.430 g, 0.599 mmol, 64%). X-ray-quality crystals of **3a** were grown upon cooling the washings to −30 °C (see Table 14 for selected bond lengths and angles). Total yield: 47%. Color: red-orange. MS (LSI$^+$, *m*-NBA): *m*/*z* 718.2585 ([M]$^+$, 30%), *m*/*z* calc for [$C_{46}H_{48}P_2{}^{56}Fe$]$^+$ = 718.2581. Anal. Calcd for $C_{46}H_{48}P_2Fe_1$: C, 76.88; H, 6.73. Found: C, 76.84; H, 6.84. FT-IR (ν, KBr/CH_2Cl_2, cm^{-1}): 2052/2048 (s, C≡C). Raman (neat, ν, cm^{-1}): 2053 (vs, C≡C). ^{31}P{^{1}H} NMR (C_6D_6, 81 MHz, δ in ppm): 101.7 (s, dppe). ^{1}H NMR (C_6D_6, 200 MHz, δ in ppm): 8.06 (m, 4H, $H_{ortho/Ph1/dppe}$); 7.29−6.94 (m, 18H, $H_{Ar/dppe}$ + H_{oMes}); 6.67 (s, 1H, H_{pMes}); 2.70 (m, 2H, CH_{2dppe}); 2.19 (s, 6H, 2CH_3); 1.85 (m, 2H, CH_{2dppe}); 1.57 (s, 15H, C_5(CH_3)$_5$). ^{13}C{^{1}H} NMR (C_6D_6, 50 MHz, δ in ppm): 141.0−127.5 (m, 8$C_{Ar/dppe}$+ 2 CH$_{Mes}$); 137.2 (s, $C_{quat./Mes}$); 131.6 (s, $C_{quat./Mes}$); 136.0 (t, $^2J_{CP}$ = 40 Hz, Fe-C≡C); 125.9 (s, C-H$_{Mes}$); 121.3 (s, Fe-C≡C); 88.3 (s, C_5(CH$_3$)$_5$); 31.4 (m, CH$_{2/dppe}$); 21.2 (s, CH$_3$); 11.1 (s, C_5(CH$_3$)$_5$). CV: E_0 (ΔE_p, i_{pa}/i_{pc}) −0.19 V (0.07, 1) vs SCE. UV−vis (CH_2Cl_2): λ_{max}(ϵ/10^3 dm^3 M^{-1} cm^{-1}) 246 (sh, 28.0); 284 (sh, 13.1); 346 (12.8).

Selected Data for [(η^2-dppe)(η^5-C_5Me_5)Fe=C=CH{3,5-(C_6H_3)(CH_3)$_2$}][PF_6] (7a[PF_6]). FT-IR (ν, KBr, cm^{-1}): 1618 (s, Fe=C=C). ^{31}P{^{1}H } NMR ($CDCl_3$, 81 MHz, δ in ppm): 89.0 (s, dppe); 143.1 (septuplet, $^1J_{PF}$ = 712 Hz, PF_6^-). ^{1}H NMR (δ, $CDCl_3$, 200 MHz): 7.70−7.20 (m, 16H, $H_{Ar/dppe}$); 7.15 (m, 4H, $H_{Ar/dppe}$); 6.68 (s, 1H, H_{Mes}); 6.05 (s, 2H, H_{Mes}); 5.09 (t, $^4J_{HP}$ = 4 Hz, 1H, Fe=C=C(Ar)H); 3.08 (m, 2H, CH_{2dppe}); 2.52 (m, 2H, CH_{2dppe}), 2.04 (s, 6H, CH_3); 1.59 (s, 15H, C_5(CH_3)$_5$). ^{13}C NMR ($CDCl_3$, 50 MHz, δ in ppm): 362.7 (m, $^2J_{CP}$ = 34 Hz, $^2J_{CH}$ = 6.1 Hz, Fe=C=C); 138.0 (m, $^4J_{CH}$ = 5 Hz, $^1J_{CH}$ = 152 Hz, C-CH$_{3/Mes}$); 133.8−128.6 (m, 12C_{Ar}); 126.4 (m, $^3J_{CP}$ = 5 Hz, $^1J_{CH}$ = 152 Hz, Fe=C=C); 124.8 (d, $^1J_{CH}$ = 157 Hz, CH$_{Mes}$); 100.5 (s, C_5(CH$_3$)$_5$); 29.4 (m, CH$_{2/dppe}$); 21.4 (q, $^1J_{CH}$ = 126 Hz, CH$_{3/Mes}$); 10.5 (q, $^1J_{CH}$ = 128 Hz, C_5(CH$_3$)$_5$).

Synthesis of the Mononuclear Fe(II) Alkynyl Complex (η^2-dppe)(η^5-C_5Me_5)Fe−C≡C-2,4,6-(C_6H_2(CH_3)$_3$) (3b). (η^2-dppe)(η^5-C_5Me_5)Fe(Cl) (**2**, 1.000 g, 1.60 mmol), NH_4PF_6 (0.315 g, 1.93 mmol), and (2,4,6-trimethylphenyl)acetylene (0.350 g, 2.40 mmol) were suspended in 30 mL of methanol, and the mixture was stirred for 48 h at 25 °C. After concentration to 10 mL and decantation, the pale orange solid that formed was filtrated, washed with methanol (5 mL), and extracted with 50 mL of dichloromethane. Concentration of the extract (2 mL) and precipitation by excess diethyl ether (20 mL) allowed the isolation of [(η^2-dppe)(η^5-C_5Me_5)Fe=C=CH{2,4,6-(C_6H_2)(CH_3)$_3$}][PF_6] (**7b**[PF_6]) as an air-sensitive orange solid (1.256 g, 1.429 mmol, 89%). This vinylidene complex (1.000 g, 1.13 mmol) was then stirred for 12 h in THF in the presence of excess potassium *tert*-butoxide (0.193 g, 1.700 mmol). After evacuation of the solvent and extraction with toluene, concentration of the extract to dryness, and subsequent washings with *n*-pentane, the desired orange complex (η^2-dppe)(η^5-C_5Me_5)-Fe[C≡C-2,4,6-(C_6H_2)(CH_3)$_3$] (**3b**) was obtained (0.710 g, 0.965

(81) Connelly, N. G.; Geiger, W. E. *Chem. Rev.* **1996**, *96*, 877−910.
(82) Lavastre, O.; Ollivier, L.; Dixneuf, P. H.; Sinbandhit, S. *Tetrahedron* **1995**, *52*, 5495−5504.
(83) (a) Dolhem, F.; Lièvre, C.; Demailly, G. *Tetrahedron Lett.* **2002**, *43*, 1847−1849. (b) Michel, P.; Gennet, D.; Rassat, A. *Tetrahedron Lett.* **1999**, *40*, 8575−8578.

Table 14. Selected Bond Lengths (Å) and Angles (deg) for 1c[PF_6], *m*-1d[PF_6], 3a, 3b·C_6H_6, and 3b[PF_6]·C_6H_6

	1c[PF_6]	***m*-1d**[PF_6]	**3a**	**3b**·C_6H_6	**3b**[PF_6]·$^1/_2CHCl_3$
			Selected Bond Lengths		
Fe−(Cp*)$_{centroid}$	1.772	1.776	1.733	1.741	1.772
Fe−P1	2.2708(7)	2.2523(7)	2.1707(13)	2.1740(12)	2.2595(11)
Fe−P2	2.2565(7)	2.2879(7)	2.1788(14)	2.1615(13)	2.2441(10)
Fe−C37	1.896(3)	1.891(2)	1.896(5)	1.899(5)	1.885(4)
C37−C38	1.220(4)	1.207(3)	1.210(7)	1.235(6)	1.218(6)
C38−C39	1.437(4)	1.446(3)	1.455 (7)	1.444(6)	1.436(5)
C39−C40	1.400(4)	1.394(3)	1.397(7)	1.408(6)	1.416(6)
C40−C41	1.386(4)	1.383(3)	1.392(7)	1.397(6)	1.398(6)
C41−C42	1.390(4)	1.370(4)	1.379(7)	1.387(7)	1.395(7)
C42−C43	1.386(4)	1.380(4)	1.388(8)	1.393(7)	1.378(7)
C43−C44	1.385(4)	1.381(3)	1.400(7)	1.392(6)	1.397(6)
C39−C44	1.404(4)	1.405(3)	1.385(8)	1.410(6)	1.411(6)
C41−C45			1.508(8)		
C42−C45	1.497(4)				
C45−F1	1.335(4)				
C45−F1	1.337(4)				
C45−F1	1.321(4)				
C41−F1		1.365(3)			
C43−C46			1.498(9)		
C40−C45				1.503(6)	1.510(6)
C42−C46				1.504(7)	1.514(6)
C44−C47				1.502(6)	1.493(6)
			Selected Bond Angles		
P1−Fe−P2	84.31(3)	83.78(2)	84.79(5)	85.98(5)	83.80(4)
P1−Fe−C37	92.68(8)	83.74(1)	82.55(14)	85.94(13)	87.47 (11)
P2−Fe−C37	83.48(8)	90.58(7)	83.61(15)	83.22(13)	86.51(11)
Fe−C37−C38	171.9(2)	173.1(2)	176.9(4)	179.3(4)	178.6(4)
C37−C38−C39	174.8(32)	173.5(2)	171.9(5)	177.7(4)	177.4(4)
Fe−(Cp*)$_{centroid}$/C39−C40 *a*	−87.2	−97.5	−120.3	−136.36	37.9

[a] Dihedral angle (Cp* = pentamethylcyclopentadienyl ligand).

mmol, 85%). X-ray-quality crystals of **3b**·C_6H_6 were grown by slow evaporation of a benzene solution of the complex (see Table 14 for selected bond lengths and angles). Total yield: 76%. Color: red-orange. MS (LSI$^+$, *m*-NBA): *m*/*z* 718.2585 ([M]$^+$, 100%), *m*/*z* calc for [$C_{47}H_{50}P_2{}^{56}Fe$]$^+$ = 732.2737. Anal. Calcd for $C_{47}H_{50}P_2Fe_1$: C, 77.05; H, 6.88. Found: C, 76.38; H, 6.79. FT-IR (ν, KBr/CH_2Cl_2, cm^{-1}): 2036/2037 (s, C≡C). Raman (neat, ν, cm^{-1}): 2037 (vs, C≡C). $^{31}P\{^1H\}$ NMR (C_6D_6, 81 MHz, ppm, δ in ppm): 102.5 (s). ^1H NMR (C_6D_6, 200 MHz, δ in ppm): 7.92 (m, 4H, $H_{ortho/Ph1/dppe}$); 7.36 (m, 2H, H_{Mes}); 7.25−7.00 (m, 16H, $H_{Ar/dppe}$); 2.87 (m, 2H, CH_{2dppe}); 2.22 (s, 3H, CH_3); 2.13 (s, 6H, 2CH_3); 1.92 (m, 2H, CH_{2dppe}); 1.57 (s, 15H, C_5(CH_3)$_5$). $^{13}C\{^1H\}$ NMR ($CDCl_3$, 50 MHz, δ in ppm): 141.0−127.5 (m, 8$C_{Ar/dppe}$ + 2 $CH_{Ar/Mes}$ + $C_{Ar/Mes}$; + Fe−*C*≡C); 139.2 (s, $C_{quat./Mes}$); 131.1 (s, $C_{quat./Mes}$); 118.9 (s, Fe−C≡*C*); 87.9 (s, C_5(CH$_3$)$_5$); 31.0 (m, $CH_{2/dppe}$); 21.6 (s, 2 *C*H$_3$); 21.5 (s, *C*H$_3$); 10.7 (s, C_5(*C*H$_3$)$_5$). CV: E_0 (ΔE_p, i_{pa}/i_{pc}) −0.22 V (0.08, 1) vs SCE. UV−vis (CH_2Cl_2): λ_{max} (ϵ/10^3 dm^3 M^{-1} cm^{-1}) 352 (14.2); 496 (0.7).

Selected Data for [(η^2-dppe)(η^5-C_5Me_5)Fe=C=CH{2,4,6-(C_6H_2)(CH_3)$_3$}][PF_6] (7b[PF_6]). FT-IR (ν, KBr, cm^{-1}): 1632 (s, Fe=C=C). $^{31}P\{^1H\}$ NMR ($CDCl_3$, 81 MHz, δ in ppm): 92.5 (s, dppe); 143.1 (septuplet, $^1J_{PF}$ = 713 Hz, PF_6^-). ^1H NMR ($CDCl_3$, 200 MHz, δ in ppm): 7.65−7.00 (m, 20H, $H_{Ar/dppe}$); 6.77 (m, 2H, H_{Mes}); 5.01 (t, $^4J_{HP}$ = 4.2 Hz, 1H, C=C(Ar)*H*); 2.93 (m, 2H, CH_{2dppe}); 2.55 (m, 2H, CH_{2dppe}), 2.28 (s, 3H, CH_3); 1.71 (s, 6H, CH_3); 1.56 (s, 15H, C_5(CH_3)$_5$).

General Procedure for the Synthesis of the Mononuclear Fe(III) Alkynyl Complexes. A 0.95 equiv. portion of [Fe(η^5-C_5H_5)$_2$]-[PF_6] (0.120 g, 0.361 mmol) was added to a solution of the corresponding Fe(II) parent (0.380 mmol) in 15 mL of dichloromethane, resulting in an instantaneous darkening of the solution. Stirring was maintained 1 h at room temperature, and the solution was concentrated in vacuo to approximatively 5 mL. Addition of 50 mL of *n*-pentane allowed precipitation of a dark solid. Decantation and subsequent washings with 3 × 3 mL portions of toluene followed by 3 × 3 mL of diethyl ether and drying under vacuum yielded the desired complex [(η^2-dppe)(η^5-C_5Me_5)Fe−C≡C-4-(C_6H_4)X][PF_6] as an analytically pure sample.

[(η^2-dppe)(η^5-C_5Me_5)Fe−C≡C-3,5-(C_6H_4(CH_3)$_2$)][PF_6] (3a-[PF_6]). Yield: 96%. Color: red-orange. Anal. Calcd for $C_{46}H_{48}P_3F_6Fe_1$: C, 63.97; H, 5.60; F, 13.20. Found: C, 62.90; H, 5.64; F, 13.27. FT-IR (ν, KBr/CH_2Cl_2, cm^{-1}): 1999 (vw, C≡C), 1951 (sh)/1998 (m, C≡C). Raman (neat, ν, cm^{-1}): 1949 (vw, C≡C). ESR (77 K): g_1 = 1.981, g_2 = 2.056, g_3 = 2.455. UV−vis (CH_2Cl_2): λ_{max}(ϵ/10^3 dm^3 M^{-1} cm^{-1}) 252 (45.4); 340 (sh, 6.7); 587 (2.3); 681 (3.8).

[(η^2-dppe)(η^5-C_5Me_5)Fe−C≡C-2,4,6-(C_6H_2(CH_3)$_3$)][PF_6] (3b-[PF_6]). Yield: 94%. Color: red-brown. Anal. Calcd for $C_{47}H_{50}P_3F_6Fe_1$: C, 64.32; H, 5.74; F, 12.99. Found: C, 64.02; H, 5.66; F, 12.47. IR (KBr/CH_2Cl_2, ν, cm^{-1}): 1990/1986 (s, C≡C), 1957/1954 (w, C≡C). Raman (neat, ν, cm^{-1}): 1990 (s, C≡C), 1960 (w, C≡C). ESR (77 K): g_1 = 1.983, g_2 = 2.032, g_3 = 2.420. UV−vis (λ_{max}, CH_2Cl_2, ϵ/10^3 dm^3 M^{-1} cm^{-1}): 316 (sh, 20.3); 394 (sh, 6.7); 616 (4.4); 714 (11.8). X-ray-quality crystals of **3b**[PF_6] were grown by slow evaporation of a $CHCl_3$ solution of the compound (see Table 14 for selected bond lengths and angles).

[(η^2-dppe)(η^5-C_5Me_5)Fe−C≡C-3-(C_6H_4)F][PF_6] (*m*-1d[PF_6]). Yield: 78%. Color: brown. Anal. Calcd for $C_{44}H_{43}F_7P_3Fe_1$: C, 61.89; H, 5.08. Found: C, 61.95; H, 5.14. FT-IR (KBr/CH_2Cl_2, ν, cm^{-1}): 2012 (w, C≡C)/2016 (vw, C≡C). ESR (77 K): g_1 = 1.975, g_2 = 2.030, g_3 = 2.454. X-ray-quality crystals of ***m*-1d**[PF_6] were grown by slow diffusion of *n*-pentane in a CH_2Cl_2 solution of the complex (see Table 14 for selected bond lengths and angles).

Computational Details. DFT calculations were carried out using the Amsterdam density functional ADF 2004.01 program[84] on the model compounds $(PH_3)_2$(η^5-C_5H_5)Fe(C≡C-4-C_6H_4X)$^+$ (X = NO_2, H, Me, NH_2) and on the real compounds (η^2-dppe)(η^5-C_5Me_5)Fe-(C≡C-4-C_6H_4X)$^+$ (X = NO_2, Me). Electron correlation was treated within the local density approximation (LDA) in the Vosko−Wilk−Nusair parametrization.[85] The nonlocal corrections of Becke[86] and

(84) (a) te Velde, G.; Bickelhaupt, F. M.; Fonseca, Guerra, C.; van Gisbergen, S. J. A.; Baerends, E. J.; Snijders, J.; Ziegler, T. *Theor. Chem. Acc.* **2001**, *22*, 931−967. (b) Fonseca, Guerra, C.; Snijders, J.; te Velde, G.; Baerends, E. J. *Theor. Chem. Acc.* **1998**, *99*, 391−403. (c) *ADF2.3* and *ADF2002.01*; Theoretical Chemistry, Vrije Universiteit: Amsterdam, The Netherlands, SCM.

Table 15. Crystal Data, Data Collection, and Refinement Parameters for 1c[PF_6], *m*-1d[PF_6], 3a, 3b·C_6H_6, and 3b[PF_6]·1/2$CHCl_3$

	1c[PF_6]	***m*-1d**[PF_6]	**3a**	**3b**·C_6H_6	**3b**[PF_6]·1/2$CHCl_3$
formula	$C_{45}H_{43}F_9P_3Fe_1$	$C_{44}H_{43}F_7P_3Fe_1$	$C_{46}H_{48}P_2Fe_1$	$C_{47}H_{50}P_2Fe_1 \cdot C_6H_6$	$C_{47}H_{50}P_2Fe_1,PF_6 \cdot 1/2CHCl_3$
fw	903.55	853.54	718.63	810.77	937.31
temp (K)	120(1)	100(1)	120(1)	120(1)	120(1)
cryst syst	orthorhombic	monoclinic	triclinic	triclinic	triclinic
space group	*Pbcn*	$P2_1$	$P\bar{1}$	$P\bar{1}$	$P\bar{1}$
a (Å)	16.0682(5)	9.5078(4)	8.5747(5)	10.6961(4)	11.0094(3)
b (Å)	12.2876(4)	16.2192(6)	11.7050(7)	11.0582(3)	15.0407(3)
c (Å)	42.3400(10)	13.2545(6)	19.2720(10)	20.3047(8)	15.8834(3)
α (deg)	90.00(0)	90.00(0)	88.957(3)	80.010(2)	67.975(1)
β (deg)	90.00(0)	106.059(3)	83.951(3)	86.082(2)	79.233(1)
γ (deg)	90.00(0)	90.00(0)	79.234(2)	64.282(2)	74.729(1)
V (Å^3)	8359.6(2)	1964.2(1)	1889.6(2)	2130.8(2)	2340.7(1)
Z	8	2	2	2	2
D_{calcd} (g cm^{-3})	1.436	1.443	1.263	1.264	1.330
cryst size (mm)	0.35 × 0.25 × 0.22	0.22 × 0.12 × 0.10	0.22 × 0.12 × 0.12	0.22 × 0.22 × 0.18	0.45 × 0.32 × 0.32
F(000)	3720	882	760	860	972
diffractometer	Oxford Diffraction Xcalibur Saphir 3		KappaCCD (Nonius)	KappaCCD (Nonius)	KappaCCD (Nonius)
radiation	Mo Kα	Mo Kα	Mo Kα	Mo Kα	Mo Kα
abs coeff (mm^{-1})	0.548	0.572	0.515	0.465	0.566
data collection: θ_{max} (deg)	54	54	60	54	54
frames			1145	210	210
Ω rotation (deg)	0.7	0.7	0.3	1.5	2.0
seconds/frame	20	20	12	30	10
θ range	2.71−32.22	2.98−32.26	1.06−27.65	1.02−27.56	1.39−27.50
h k l range	−23/23	−13/14	0/11	−13/13	0/14
	−10/18	−16/23	−14/15	−14/14	−18/19
	−60/62	−19/19	−24/24	−26/67	−19/20
no. total reflns	75 304	19 221	16 215	28 978	42 484
no. unique reflns	13 873	9134	7942	9705	10 730
no. obsd reflns [$I > 2\sigma(I)$]	8428	6764	5867	6589	8193
no. restraints/params	0/526	0/496	0/443	0/560	0/550
$w = 1/[\sigma^2(F_o)^2 + (aP)^2 + bP]$	$a = 0.0745$	$a = 0.0370$	$a = 0.0904$	$a = 0.057$	$a = 0.1451$
(where $P = [F_o^2 + F_c^2]/3$)	$b = 6.9722$	$b = 0.0000$	$b = 5.4105$	$b = 6.66$	$b = 6.0134$
final *R*	0.065	0.033	0.087	0.072	0.081
R_w	0.155	0.068	0.206	0.180	0.225
R indices (all data)	0.109	0.053	0.123	0.113	0.105
R_w (all data)	0.165	0.071	0.236	0.201	0.251
goodness of fit/F^2 (S_w)	1.050	0.892	1.139	1.082	1.057
$\Delta\rho_{max}$ (e Å^{-3})	1.711	0.402	0.619	0.539	2.314
$\Delta\rho_{min}$ (e Å^{-3})	−1.251	−0.385	−0.818	−0.568	−1.015

of Perdew[87] were added to the exchange and correlation energies, respectively. The numerical integration procedure applied for the calculations was developed by te Velde et al.[85] The basis set used for the metal atom was a triple-ζ Slater-type orbital (STO) basis for Fe 3d and 4s and a single-ζ function for Fe 4p. A triple-ζ STO basis set was employed for H 1s and for 2s and 2p of C, N, and O, extended with a single-ζ polarization function (2p for H; 3d for C, N, and O). Full geometry optimizations (assuming C_1 symmetry) were carried out on each complex, using the analytical gradient method implemented by Verluis and Ziegler.[88] For compound **1f**-H^+ (X = H), no local minimum was found for the perpendicular conformation and the C_s symmetry was imposed. The energy difference between these conformers is therefore meaningless and was not reported. Spin-unrestricted calculations were performed for all the considered open-shell systems. Representations of the molecular orbitals were done using MOLEKEL4.1.[89]

Crystallography. Crystals of **1c**[PF_6], ***m*-1d**[PF_6], **3a**, **3b**·C_6H_6, and **3b**[PF_6]·$^1/_2CHCl_3$ were obtained as described above. The samples were studied on an Oxford Diffraction Xcalibur Saphir 3 or on a NONIUS Kappa CCD with graphite-monochromatized Mo Kα radiation. The cell parameters were obtained with Denzo and Scalepack with 10 frames (psi rotation: 1° per frames).[90] The data collection[91] ($2\theta_{max}$, number of frames, Ω rotation, scan rate, and HKL range as given in Table 14) provided reflections for **1c**[PF_6], ***m*-1d**[PF_6], **3a**, **3b**·C_6H_6, and **3b**[PF_6]·$^1/_2CHCl_3$. Subsequent data reduction with Denzo and Scalepack[90] gave the independent reflections (Table 15). The structures were solved with SIR-97, which revealed the non-hydrogen atoms.[92] After anisotropic refinement, the remaining atoms were found in Fourrier difference maps. The complete structures were then refined with SHELXL97[93] by the full-matrix least-squares technique (use of F^2 magnitude; *x*, *y*, *z*, β_{ij} for Fe, P, C, N, and/or O atoms, *x*, *y*, *z* in riding mode for H atoms with variables "*N*(var.)", observations and "*w*" used as

(85) Vosko, S. D.; Wilk, L.; Nusair, M. *Can. J. Chem.* **1990**, *58*, 1200−1211.

(86) (a) Becke, A. D. *J. Chem. Phys.* **1986**, *84*, *4524*−4529. (b) Becke, A. D. *Phys. Rev. A* **1988**, *38*, 3098−3100.

(87) (a) Perdew, J. P. *Phys. Rev. B* **1986**, *33*, *8822*−8824. (b) Perdew, J. P. *Phys. Rev. B* **1986**, *34*, 7406.

(88) Versluis, L.; Ziegler, T. *J. Chem. Phys.* **1988**, *88*, 322−328.

(89) Flükiger, P.; Lüthi, H. P.; Portmann, S.; Weber, J. *MOLEKEL4.1*; Swiss Center for Scientific Computing (CSCS): Switzerland, 2000−2001.

(90) Otwinowski, Z.; Minor, W. In *Methods in Enzymology*; Carter, C. W., Sweet, R. M., Eds.; Academic Press: London, 1997; Vol. 276, pp 307−326.

(91) Nonius, B. V. *Kappa CCD Software*; Delft: The Netherlands, 1999.

(92) Altomare, A.; Burla, M. C.; Camalli, M.; Cascarano, G.; Giacovazzo, C.; Guagliardi, A.; Moliterni, A. G. G.; Polidori, G.; Spagna, R. *J. Appl. Chem.* **1998**, *31*, 74−77.

(93) Sheldrick, G. M. *SHELX97*-2, Program for the refinement of crystal structures; Univ. of Göttingen: Germany, 1997.

defined in Table 15). Atomic scattering factors were taken from the literature.[94] ORTEP views of **1c**$^+$, ***m*-1d**$^+$, **3a**, and **3b**$^+$ were realized with PLATON98.[95]

Acknowledgment. F.P. and N.G. thank Region Bretagne for financial support. The CNRS is also acknowledged for financial support and the Institut de Développement et de Ressources en Informatique (IDRIS, Orsay) for computing facilities.

(94) Reidel, D. *International Tables for X-ray Crystallography*; Kynoch Press (present distrib. D. Reidel, Dordrecht): Birmingham, 1974; Vol. IV.
(95) Spek, A. L. *PLATON, A Multipurpose Crystallographic Tool*; Utrecht University: Utrecht, The Netherlands, 1998.

Supporting Information Available: Experimental details about the NMR measurements (pulse widths, etc.), ^{1}H NMR shifts vs Fe(II)/Fe(III) ratios in CD_2Cl_2 at 25 °C for **1g**/**1g**[PF_6] and **2**/**2**[PF_6], additional details regarding the assignment of the ^{1}H and ^{13}C NMR shifts, COSY, HMQC, and NOESY spectra for selected compounds, T_1 measurements for **1a**[PF_6] and **1b**[PF_6], half-width data for selected compounds, Solomon−Bloembergen treatment of ^{1}H NMR relaxation, selected correlations, and CIF files for **1c**[PF_6], ***m*-1d**[PF_6], **3a**, **3b**·C_6H_6, and **3b**[PF_6]·$CDCl_3$. This material is available free of charge via the Internet at http://pubs.acs.org.

OM060989J